



THE HONG KONG
POLYTECHNIC UNIVERSITY

香港理工大學

Pao Yue-kong Library

包玉剛圖書館

Copyright Undertaking

This thesis is protected by copyright, with all rights reserved.

By reading and using the thesis, the reader understands and agrees to the following terms:

1. The reader will abide by the rules and legal ordinances governing copyright regarding the use of the thesis.
2. The reader will use the thesis for the purpose of research or private study only and not for distribution or further reproduction or any other purpose.
3. The reader agrees to indemnify and hold the University harmless from and against any loss, damage, cost, liability or expenses arising from copyright infringement or unauthorized usage.

IMPORTANT

If you have reasons to believe that any materials in this thesis are deemed not suitable to be distributed in this form, or a copyright owner having difficulty with the material being included in our database, please contact lbsys@polyu.edu.hk providing details. The Library will look into your claim and consider taking remedial action upon receipt of the written requests.

**INVESTIGATION AND REMEDIATION OF
FALSE TOPOGRAPHIC PERCEPTION PHENOMENA
OBSERVED ON LUNAR ORBITAL IMAGERY**

GAO YANG

M.Phil

The Hong Kong Polytechnic University

2013

The Hong Kong Polytechnic University

Department of Land Surveying & Geo-Informatics

**INVESTIGATION AND REMEDIATION OF FALSE
TOPOGRAPHIC PERCEPTION PHENOMENA OBSERVED ON
LUNAR ORBITAL IMAGERY**

GAO Yang

A thesis submitted in partial fulfilment of the requirements for

the degree of Master of Philosophy

January 2012

Certificate of Originality

I hereby declare that this thesis is my own work and that, to the best of my knowledge and belief, it reproduces no material previously published or written, nor material that has been accepted for the award of any other degree or diploma, except where due acknowledgement has been made in the text.

_____ (Signed)

_____ GAO YANG _____ (Name of student)

Abstract

False Topographic Perception Phenomenon (FTPP) is a relief inversion phenomenon in remote sensing images and causes false perception problems, for example, craters appear as hillocks, mountains appear as valleys, and vice versa. Such images of the Moon suffer from serious FTPP problems. This is mainly due to the highly rugged and dust grayout surface, the absence of atmosphere eliminates the scattering effects, and the lack of familiar landmarks on the Moon, to supply visual cues. Correctly observing and understanding the terrain features on the Moon from lunar surface images is important for lunar exploration missions and various lunar scientific investigations. Therefore, this study systematically investigates the FTPP problem observed on lunar orbiter imagery (mainly based on the Chinese Chang'E-1 imagery) and develops methods to alleviate the FTPP problem on lunar orbiter imagery.

Firstly, a systematic investigation of the FTPP problem observed on the Chang'E-1 imagery was performed. The Chang'E-1 images covering the whole lunar surface was examined, and terrain features (mainly craters) suffer from obvious FTPP problems were identified. Results revealed that the FTPP problem is positively correlated to the latitude of the terrain features, and majority of the objects suffering from the FTPP problem on the Chang'E-1 imagery are in the north hemisphere. For craters within a similar latitude range, the FTPP level is positively correlated with

the depth-diameter ratio of the crater. Other factors related to the FTTP problem was analyzed, such as the sun elevation and azimuth angles, observation angles, and influence of shadows.

Secondly, several traditional methods were investigated to alleviate the FTTP problem, which included the method of image rotation and the Digital Number (DN) invert method. Experimental results showed that these traditional methods have advantages as well as disadvantages when dealing with lunar orbiter imagery.

Thirdly, this study develops two approaches for FTTP remediation on Chang'E-1 imagery. One is a wavelet-transform based approach. Digital terrain models of several craters were generated from the Chang'E-1 imagery based on Photogrammetric techniques, and SRMs with specific light directions were derived. Data fusion was then performed among the original image and the Shadowed Relief Model (SRM) using the Shift Invariance Discrete Wavelet Transform (SIDWT) method. After that, images free of FTTP can be obtained. The other is a rotation-invariant approach, in which an illumination balanced image was firstly generated and then a bright-darker depth map was incorporated to generate images free of FTTP. Experimental analysis using three different types of craters revealed that both methods are able to effectively correct the FTTP problem, while the wavelet-transform based approach is only recommended for circumstances with no image rotation. The rotation-invariant approach, however, is not subject to image rotation

and is suitable for applications such as those using the lunar surface images for navigation or exploring lunar surface using software systems such as Google Moon.

Acknowledgment

I would like to take this chance to express my sincere gratitude to my supervisor, Dr. Bo Wu, who gives me many kindly assistance and valuable suggestions during the process of my thesis writing. His willingness to give his time so generously has been very much appreciated.

My gratitude also extends to the co-supervisor Prof. Zhilin Li for his kind encouragement and patient instructions.

Last but not the least, I would like to offer my particular thanks to my dear senior classmates Guo Jian, Li Haifeng and my family, for their encouragement and support for the completion of this thesis.

Table of Contents

CERTIFICATE OF ORIGINALITY	1
ABSTRACT	2
ACKNOWLEDGMENT	5
TABLE OF CONTENTS	6
LIST OF FIGURES	9
LIST OF TABLES	13
CHAPTER 1 INTRODUCTION	14
1.1 RESEARCH BACKGROUND	14
1.2 RESEARCH OBJECTIVES	17
1.3 RESEARCH PROBLEM STATEMENT AND RESEARCH SIGNIFICANCE	18
1.4 LITERATURE REVIEW	19
CHAPTER 2 INVESTIGATION OF FTTP OBSERVED ON CHANG’E-1 IMAGERY	28
2.1 OBSERVATION OF FTTP ON CHANG’E-1 IMAGERY	28
2.2 ANALYSIS OF FACTORS RELATED TO FTTP PROBLEMS	35
<i>2.2.1 Relationship between FTTP and Object Locations</i>	35
<i>2.2.2 Relationship between FTTP and Crater Shapes</i>	39

2.2.3 <i>Other Factors Related to FTTP</i>	43
CHAPTER 3 REMEDIATION OF FTTP ON LUNAR IMAGERY	48
3.1 TRADITIONAL METHODS	48
3.1.1 <i>Image Rotation</i>	48
3.1.2 <i>Digital Number Value Inversion</i>	53
3.2 A WAVELET-TRANSFORM BASED APPROACH FOR FTTP REMEDIATION ON LUNAR IMAGERY	56
3.2.1 <i>Digital Elevation Model (DEM) and SRM Generation</i>	57
3.2.2 <i>Image Fusion Based on the Shift Invariance Discrete Wavelet Transform (SIDWT)</i>	66
3.3 A ROTATION INVARIANT APPROACH FOR ALLEVIATION OF FTTP PROBLEMS ON LUNAR IMAGERY	70
3.3.1 <i>Motivation and Overview of the Approach</i>	70
3.3.2 <i>Illumination Balance</i>	74
3.3.3 <i>FTTP Remediation Invariant to Image Rotation</i>	76
CHAPTER 4 FURTHER EXPERIMENTS AND EVALUATION	78
4.1 FURTHER EXPERIMENTS	78
4.1.1 <i>Crater 2</i>	78
4.1.2 <i>Crater 3</i>	84
4.2 EVALUATION	90
CHAPTER 5 CONCLUSIONS AND DISCUSSION	93
5.1 CONCLUSIONS	95

5.2 DISCUSSION AND FUTURE WORK..... 96

REFERENCES..... 99

APPENDIX I..... 103

APPENDIX II..... 108

List of Figures

Figure 1.1 Examples of FTPP observed on lunar orbiter imagery.....	16
Figure 1.2 Symmetrical array about horizontal axis.....	21
Figure 1.3 Original image of study area in India.....	24
Figure 1.4 FTPP remediated image of study area in India by using SRM transformation.....	25
Figure 2.1 The Chang'E-1 imagery covering the whole lunar surface and the distribution of the selected 26 tracks.....	29
Figure 2.2 Distributions of the craters suffering from obvious FTPP problems in the Chang'E-1 imagery.....	30
Figure 2.3 Apollo 15 landing site.....	34
Figure 2.4 A typical crater in median size.....	34
Figure 2.5 Crater Aristillus.....	35
Figure 2.6 Histograms of craters suffering from FTPP with latitude.....	36
Figure 2.7 Histograms of craters suffering from FTPP with longitude.....	36
Figure 2.8 Histograms of the craters with respect to different FTPP levels.....	41

Figure 2.9 Histograms of the craters with respect to different ranges of crater shape ratio I	41
Figure 2.10 Distribution of FTPP levels with respect to crater shapes of all examined crater.....	42
Figure 2.11 Distribution of FTPP levels with respect to crater shapes with RMS of I in each FTPP level.....	43
Figure 2.12 A crater at different illumination azimuth angles and viewing angles..	44
Figure 2.13 SRMs of median size cater with azimuth angle of 225 degrees and various sun elevation angles.....	46
Figure 2.14 SRMs of a large size cater with azimuth angle of 225 degrees and various sun elevation angles.....	47
Figure 3.1 A Crater with the FTPP problem in track 0435.....	49
Figure 3.2 A Crater without the FTPP problem in track 0435.....	49
Figure 3.3 Hadley C.....	51
Figure 3.4 Part of Rima Hadley.....	52
Figure 3.5 Crater Aristillus treated by DN Inversion.....	54
Figure 3.6 Crater 1 treated by DN Inversion.....	55
Figure 3.7 Overview of the wavelet-transform based approach.....	56

Figure 3.8 Interface of control points selection.....	58
Figure 3.9 Interface of parameter setting.....	59
Figure 3.10 Interface of points digitization.....	60
Figure 3.11 Interface of DEM extraction.....	61
Figure 3.12 DEMs of Crater 1.....	62
Figure 3.13 SRMs of Crater 1.....	64
Figure 3.14 Flowchart of SIDWT.....	68
Figure 3.15 Fusion results image of crater 1 using the wavelet-transform based approach	69
Figure 3.16 Depth perception aided with shade.....	72
Figure 3.17 Symmetry structure with rotation invariant	72
Figure 3.18 Overview of the rotation-invariant approach.....	74
Figure 3.19 Illumination Balanced Image of crater 1.....	75
Figure 3.20 FTPP remediation of crater 1 using the rotation invariant approach...	77
Figure 4.1 Crater 2 and DEMs.....	79
Figure 4.2 SRMs of Crater 2 generated based on the DEM.....	80
Figure 4.3 Fusion result images of Crater 2.....	81

Figure 4.4 Illumination balanced result of Crater 2.....	82
Figure 4.5 FTTP remediation result of Crater 2 by using the rotation invariant approach	83
Figure 4.6 Crater 3 and DEMs.....	85
Figure 4.7 SRMs of Crater 3 generated based on the DEM.....	86
Figure 4.8 Fusion result images of Crater 3.....	87
Figure 4.9 Illumination balanced result of Crater 3.....	88
Figure 4.10 FTTP remediation result of Crater 3 by using the rotation invariant approach	89

List of Tables

Table 2.1 Examples of the recorded information of the objects with FTPP.....32

Table 2.2 Summary of the craters with FTPP problems observed on Chang'E-1
imagery.....33

Table 2.3 Sample of data collection.....39

Table 4 Summary of the survey outputs.....91

Chapter 1 Introduction

1.1 Research Background

False Topographic Perception Phenomenon (FTPP) is a relief inversion problem in remote sensing images and causes false perception phenomenon, for example, craters appear as hillocks, mountains appear as valleys, and vice versa. The FTTP problem is common with images acquired from Sun-synchronous satellite (e.g. Landsat, SPOT, QuickBird, IKONOS etc.). When a Sun-synchronous remote sensing satellite takes an image (normally in the hours around 10:30 A.M. local time) of a rugged terrain of the Earth, the FTTP is observed. This effect can also be seen in the Shaded Relief Models (SRMs) if they are generated with illumination sources direction other than from north-west. Saraf et al. (1996) have first identified this FTTP in the images of the Earth acquired from Sun-synchronous satellite and suggested a few correction methods (Saraf et al., 1996; 2003; 2007). Rudnicki (2000) also discussed inverse topographic perception in SRMs. Patterson (2004) described FTTP as “relief inversion”. The southeast lighting (lower right) found on most satellite images causes an optical illusion known as relief inversion, whereby mountains appear as valleys and vice versa, when the image is viewed keeping north upward (Patterson, 2004).

The FTTP problem has also been noticed on lunar images (Saraf et al., 2011). Actually, remote sensing images of the Moon surface suffer from more serious FTTP problems. This is mainly due to the highly rugged and dust grayout surface, the absence of atmosphere eliminated the scattering effects, and the lack of familiar landmarks as visual cues on the Moon (Colby, 1991; Rieser et al., 1995). Figure 1.1 illustrates typical examples of lunar images suffering from FTTP problems. Figure 1.1 (a) shows a crater in the Chinese Chang'E-1 image recognized as a hillock. After the image was rotated by 180, it appeared as a crater free of FTTP as shown in Figure 1.1 (b). Figure 1.1 (c) shows an example of the India Chandrayaan-1 image where a crater suffers from the FTTP problem. After the image was rotated by 180, it appeared as a crater free of FTTP as shown in Figure 1.1 (d). Figure 1.1 (e) and (f) show other similar examples as observed in NASA's Lunar Reconnaissance Orbiter (LRO) Narrow Angle Camera (NAC) images. These images were taken by different sensors at different time slots, and have different spatial resolutions, such as 120 m/pixel for the Chang'E-1 imagery (Ouyang et al., 2010), 5 m/pixel for the Chandrayaan-1 imagery (Kumar and Chowdhury, 2005), and 0.5 m/pixel for the LRO NAC imagery (Robinson et al., 2010). This indicates that the FTTP problem is quite common in lunar surface images from different sources with different resolutions.

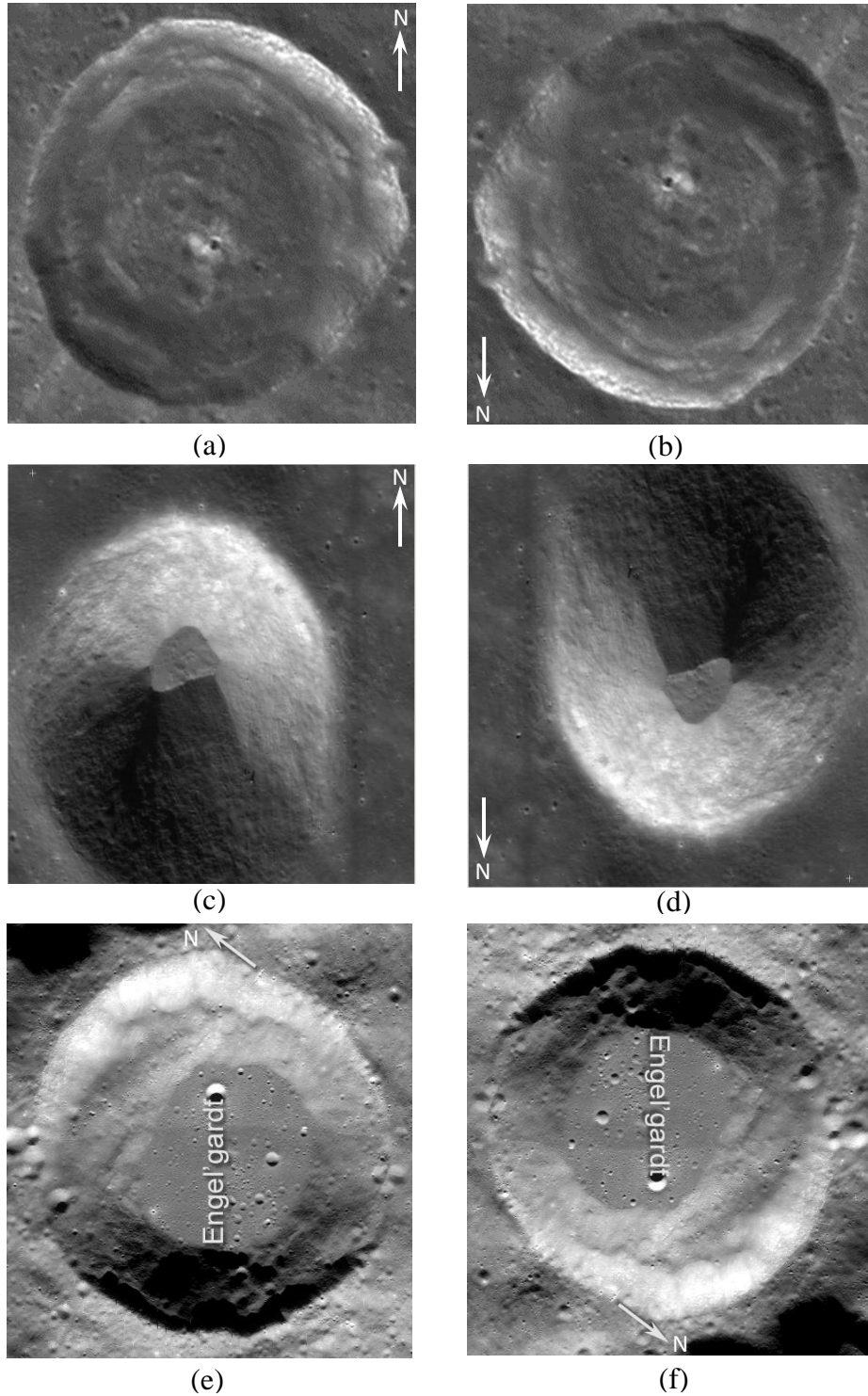


Figure 1.1 Examples of FTTP observed on lunar orbiter imagery: (a) An original Chang'E-1 image with FTTP, (b) the Chang'E-1 image rotated by 180° free of FTTP, (c) an original Chandrayaan-1 image, (d) the Chandrayaan-1 image rotated by 180° free of FTTP, (e) an original LRO image, and (f) the LRO image rotated by 180° free of FTTP.

Many factors lead to the FTPP problem such as topographic relief, object locations, sun elevation and azimuth angles, viewing angle, and hatching or engraving features present on the valley slopes (Saraf et al., 2005). Liu and Todd (2004) and Saraf et al. (2005; 2007) provided several solutions for FTPP on Earth surface images. However, this problem has not been investigated systematically, in particular for lunar orbiter imagery. There are about half a million craters with diameter greater than 1 km on the Moon (Ivanov, 2001). Correctly observing and understanding the terrain features on the lunar surface from lunar orbiter images is very important for all kinds of analysis and applications using lunar surface data. Lunar images with FTPP problems inhibit accurate scientific study of the Moon. The subsequent unreliability of the lunar surface data presents serious problems when using such evidence to support lunar robotic or human exploration missions. Hence systematic investigation of the FTPP problem in lunar surface imagery is of significant importance. Alleviation of the FTPP problem is vital to support future lunar exploration missions and various lunar scientific investigations.

1.2 Research Objectives

This research aims at systematically investigate the FTPP problem observed on the imagery of the Moon's surface and develop effective methods to alleviate the the FTPP problem. The research objectives include:

1. To systematically investigate the FTPP problem based on the Chang'E-1 imagery, and explored the factors leading to the FTPP problem;
2. To develop effective methods to alleviate the FTPP problem on lunar orbiter imagery and validate the developed methods through extensive experimental analysis.

1.3 Research Problem Statement and Research Significance

In investigating the lunar surface FTPP brings various problems such as craters appear as hillocks, mountains appear as valleys, and vice versa. If researchers or users do not notice the existence of FTPP, analysis of the terrain could be misled. Even though an FTPP suffering area is identified, it is difficult to judge whether or not the individual terrain feature suffers from FTPP.

FTPP problem has not been studied systematically, especially for lunar orbiter images. The Moon's surface appears to be highly rugged with a large number of craters distributed throughout the surface. It is very important to identify the terrain features on the Moon correctly. Correctly observing and understanding the terrain features on the lunar surface from lunar orbiter images is of significant importance for lunar exploration missions and various scientific investigations.

This research is unique in the following ways:

(1) A systematic study of the FTPP problem based on the Chang'E-1 imagery covering the whole lunar surface. Particularly, the FTPP levels are analyzed with respect to the diameter/depth ratio of craters, which is novel, to our knowledge, to the field of remote sensing image analysis.

(2) Development of effective methods for FTPP remediation of lunar imagery, which include a wavelet-transform based method and a novel rotation-invariant method. The latter is hard to achieve using traditional methods.

1.4 Literature Review

It is generally recognized that psychological factors, such as perception, play a major role in remote sensing image cognition (Toutin, 1998). The main reason causing false perception problems in remote sensing images is the prior knowledge of the observers about illumination direction. Natural experience suggests that light illuminating surfaces are not from below but from above. Human vision relies heavily on lighting cues to recover 3D shape (Morgenstern et al., 2011). When estimating 3D shapes from shading, the human visual system resolves this ambiguity by relying on the prior knowledge of illumination from light-from-above.

Ramachandran (1988a) tested a series of shaded shapes, and explained some shading perception problems from his physiology view. It was found that human brains seem to accept that only one light source illuminates the whole image. The visual system also tends to assume the light comes from one natural source, namely from above. These findings account for FPHP formation. He pointed out the ambiguity of shaded shapes being perceived either pop-out or inward in certain circumstances because the brain does not know where the light will come from, causing the observer to mentally shift the light source to invert the object depth. This opinion gave the basic idea to solve the FPHP which is reversal of illumination, which are commonly used in the current remediation FPHP method. Ramachandran (1988b) also suggested the certain feature of an object could inform the brain about the illumination direction, and depths of the other object conform to this light source. This indicates that the FPHP could be influenced by certain objects. Thus the FPHP problem in the same area could be different viewing globally or locally.

Another phenomenon has been found that false perception could happen for craters and apices in the perception about axis symmetrically (Ramachandran, 1988a). Comparing Figure 1.2 (a) with Figure 1.2 (b), the former array in Figure 1.2 (a) seems to be in the symmetrical format, though array in Figure 1.2 (b) should be truly in symmetrical format about the horizontal axis in two dimensions. This phenomenon suggests that sun elevation angle of both sides should be symmetrical to the line of subsolar point. Thus two similar craters which are symmetrical to the

subsolar line should become the situation. To correct this wrong perception, FTTP remediation is necessary.

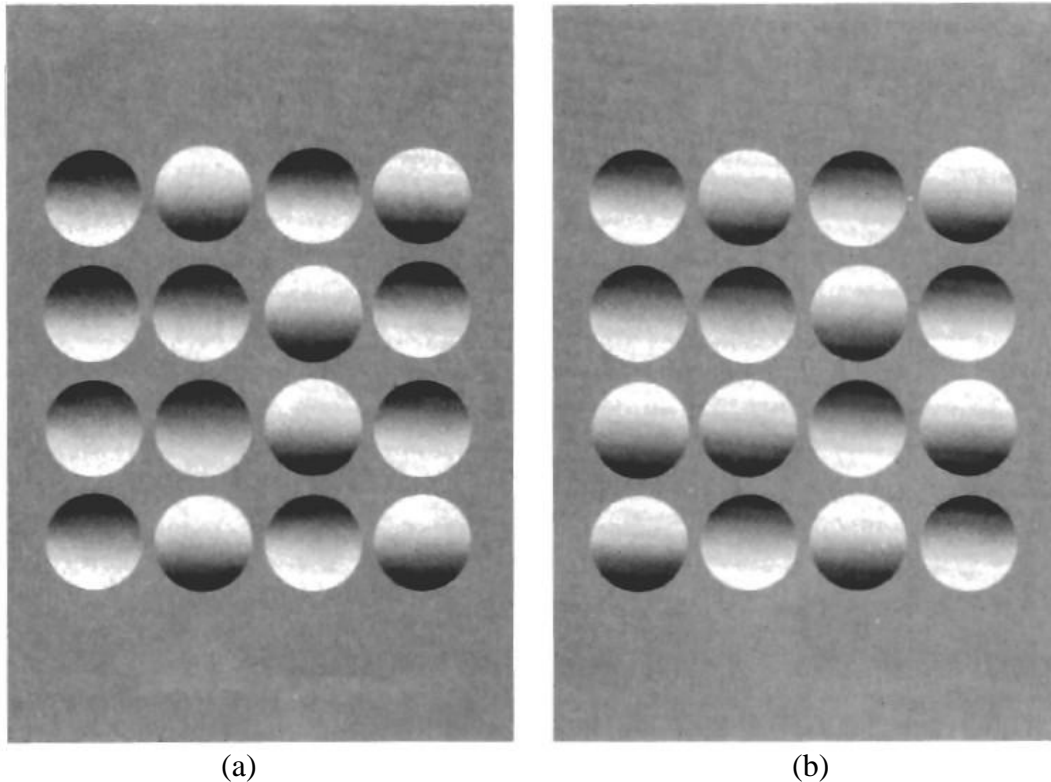


Figure 1.2 (a) Fake symmetrical array about horizontal axis; (b) true symmetrical array about horizontal axis (Ramachandran, 1988a)

Attention has been drawn to FTTP by geographers because of problems indicated in the perception of remote sensing images. Lillesand et al. (1979) noticed this during the interpretation of aerial photo images. They considered shadow plays an important role in leading this phenomenon and solving it. Patterson (2004) found this phenomenon in 2004 and named it 'Relief Inverse'. Some possible solution was also suggested such as using clone stamp tool in Photoshop to replace the shadows with neutral colours and textures. This technique, however, brings false texture

information to the image and result is poor. Meanwhile another method was suggested to use DEM to correct the shadows. But Patterson thought the DEM approach does not work because opposite light sources could eliminate the illumination while other researchers did not think so such as Saraf.

Saraf et al. (1996; 2005) analyzed the main factors leading to the FTTP problem in remote sensing images. The north-west position is always assumed by human brains of the sun-illumination position when perceiving remote sensing images. If the actual sun-illumination position deviates from the assumption when collecting remote sensing images, the FTTP problem will occur, the intensity of which will depend on the degree of deviation. Several methods have been proposed to correct the FTTP problem in remote sensing images, such as image rotation (Saraf et al., 1996), inversion of digital number (DN) value (Saraf et al., 1996), shaded relief model (SRM) and hue-intensity-saturation (HIS) transformation (Saraf et al., 2005; 2007). The core idea for all these methods is to change the illumination direction of remote sensing images to the north or above.

Image rotation refers to the rotation of the image by 180 degrees Saraf et al. (1996). This method is the easiest way to remove the FTTP impact on remote sensing imagery. However, image rotation will (1) make the north direction invert from the common, and (2) sometimes make the rotated image resemble a completely new one,

bringing new problems in image perception. Image rotation, does not correct the FTTP but hides it. When the observer again changes the view angle, a common action in certain circumstances (e.g., using the lunar surface images for navigation purposes or exploring lunar surface using software systems such as Google Moon), and the FTTP problem arises again.

DN value inversion method subtracts the grey value of each pixel by 255 to invert the DN (Digital Number) values (Saraf et al., 1996). This can avoid the inverted cartography. But the negative image here changed all the natural response from the original one, thus the image still looks different. As this method can only be used in the black and white images, it is valuable to apply it into the Chang'E-1 image data in this study to test the effect.

Using SRM (Shaded Relief Model) to solve the FTTP is another method (Saraf et al., 2005). To apply this methodology, the Digital Elevation Model (DEM) of the study area with similar spatial resolution is needed. The SRM with the same sun elevation and opposite sun azimuth (original one adds by 180 degrees) need to be produced. After that, the image in RGB format will be transformed into HIS (intensity, hue, saturation) one, and use the SRM to replace the intensity image to do the retransformation (backward from IHS to RGB). By this way, very satisfactory result can be obtained without changing the map direction or pixel value. Figure 1.3 and

Figure 1.4 show the original image and the FTTPP-remediated one obtained using this method. In Figure 1.3, the blue line which is the River Beas seems run over ridges and Pandoh Reservoir appears on the top of hills. After the SRM FTTPP remediation process, the river and reservoir are all given correct appearance as shown in Figure 1.4. The drawback of this method is that it is complex and time consuming. The DEMs and SRMs are needed. This problem could be more serious and observable for dealing with the images of dense craters. Difference of colour schemes for the original image and the resulting one is also a problem.

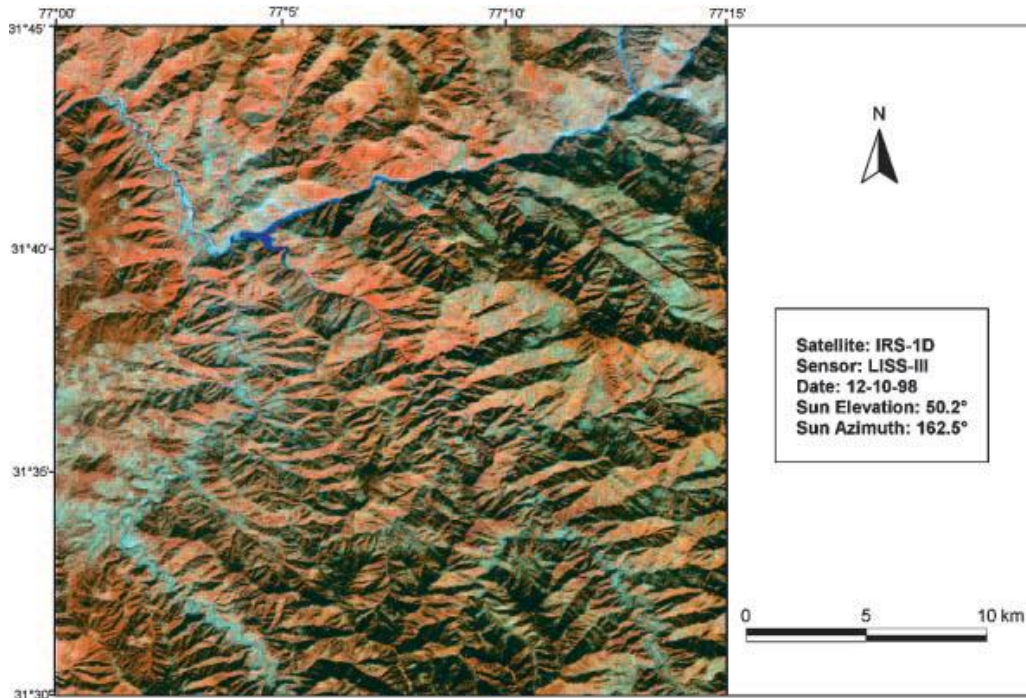


Figure 1.3 Original image of study area in India (Saraf et al., 2005).

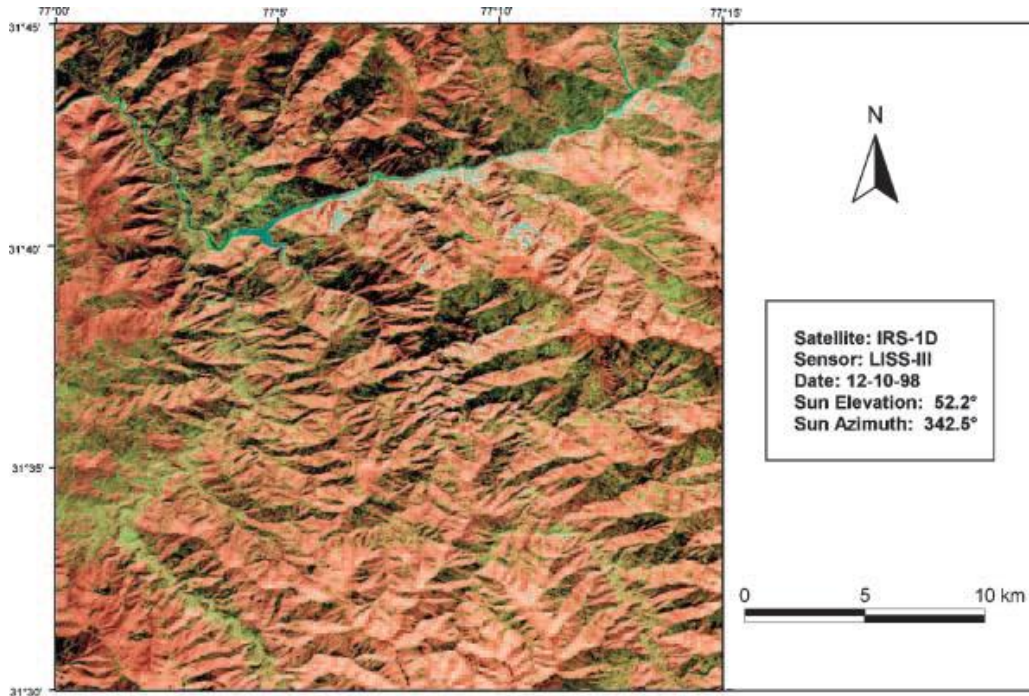


Figure 1.4 FTTP remediated image of study area in India by using SRM transformation (Saraf et al., 2005)

Saraf et al. (2007) suggested another efficient method to correct the FTTP problem. Transferred the RGB image into HIS format is the first step, then the intensity channel was inverted, and finally the image was transferred back from HIS to RGB format. This method however cannot process remote sensing images in black and white. Additionally, when inverting pixel intensity, the brightness of the image can overflow. This problem requires additional techniques to better balance the brightness, by adjusting the histogram of the intensity images.

Image fusion is a promised technique to correct the FTTP problem. Various image fusion techniques were presented in the past: intensity-hue-saturation (HIS),

principal component analysis (PCA), pixel-level multi-resolution techniques such as image pyramids, and 2D wavelet transformation (Rockinger, 1997), among which the discrete wavelet transform (DWT) technology as a kind of pixel-level image fusion techniques has been widely used in image fusion (Mallat, 1989; Rockinger, 1997). Shift invariant of the DWT (SIDWT) based method (Rockinger, 1997; Sari-Sarraf and Brzakovic, 1997) is an improved approach of it.

For pixel-level image fusion techniques, some generic requirements can be imposed on the fusion scheme: i) the fusion process should preserve all relevant information of the input imagery in the composite image sequence; ii) the fusion scheme must not introduce any artifacts or inconsistencies which would distract the human observer or the subsequent processing stages; iii) the fusion process should be shift invariant, i.e. the fusion result should not depend on the location of an object in the input imagery; iv) the fused image sequence should be temporally stable and consistent with the input sequences. The last two points are especially important in image sequence fusion (Rockinger, 1997).

In general, wavelet-based technologies (DWT, SIDWT) perform better than standard methods such as intensity-hue-saturation (HIS) and principal component analysis (PCA), particularly in terms of minimizing colour distortion [Graps, 1995; Amolins

et al., 2007]. This study employed SIDWT as the fusion method to treat the FTTP problem.

The actual fusion process in the SIDWT method is identical to that in the generic wavelet fusion case (Rockinger, 1997). The input images are decomposed into their shift invariant wavelet representation and a composite shift invariant wavelet representation is built by the incorporation of an appropriate selection scheme. For an evaluation of the different fusion methods, two selection schemes could be implemented: i) a point-based choose-max and ii) an area based selection scheme with a consistent verification follows.

Previous FTTP studies mainly focused on Earth images. FTTP problem investigations in lunar images have been seldom discussed. Investigation and remediation of the FTTP problem in lunar surface images is important for lunar scientific investigations and future lunar exploration missions since lunar surface images, as mentioned above, suffer more serious FTTP problems. Very recently, Saraf et al. (2011) demonstrated examples of serious FTTP problems as observed from the Chandrayan-1 images. However, Saraf et al. (2011) did not provide any new solution to resolve FTTP problems in lunar images.

Chapter 2 Investigation of FTTP Observed on Chang'E-1 Imagery

The Chinese Chang'E-1 lunar probe was launched on October 24, 2007. The CCD camera on-board the Chang'E-1 successfully returned 1098 orbiter images, covering the whole lunar surface. A laser altimeter which generates range measurements covering the whole Moon, is on-board the Chang'E-1. The Department of Land Surveying & Geo-Informatics (LSGI) of the Hong Kong Polytechnic University is an authorized organization of the Chang'E-1 Scientific Application Committee which can access the Chang'E-1 data. LSGI received the Chang'E-1 laser altimeter data and the Level 2C imagery from the Chang'E-1 camera in March 2009. This research mainly uses the Chang'E-1 imagery for investigation and analysis.

2.1 Observation of FTTP on Chang'E-1 Imagery

The Chang'E-1 data set used in this research is the Level 2C data released by the Chinese Academy of Sciences, which has already been processed for radiometric, geometric, and spectrophotometric correction (CAS, 2008). Since there are enormous numbers of craters on the Moon, this study focuses mainly on the FTTP

problem associated with lunar craters. Other lunar terrain features, such as valleys and mountains in lunar images may also suffer from FTTP problems. The investigations and methods presented in this paper are also useful in better enabling understanding and the subsequent solving of FTTP problems related to other lunar terrain features.

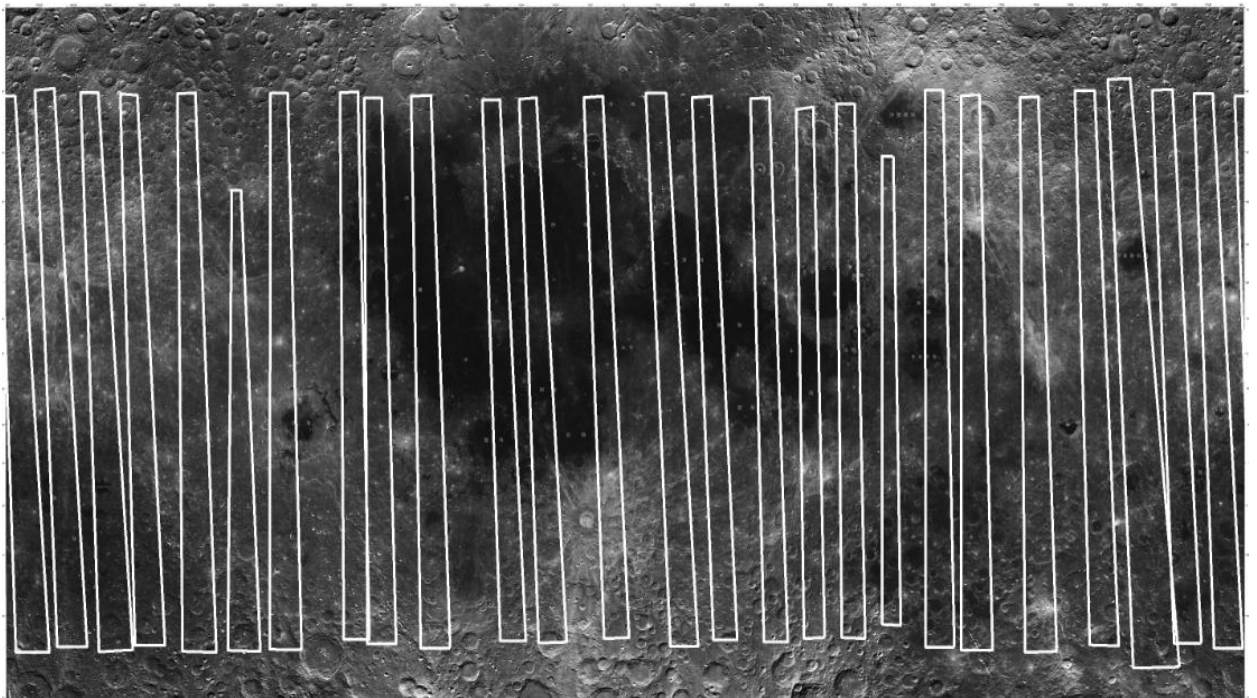


Figure 2.1 The Chang'E-1 imagery covering the whole lunar surface and the distribution of the selected 26 tracks

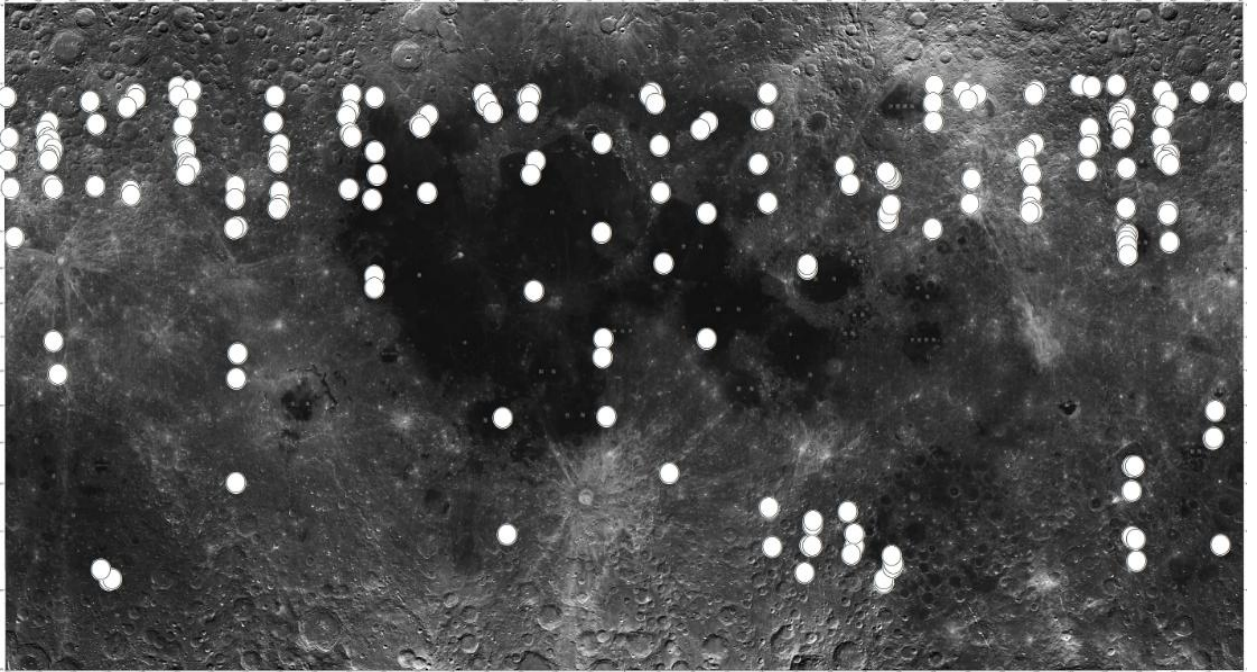


Figure 2.2 Distributions of the craters suffering from obvious FTTP problems in the Chang'E-1 imagery

Figure 2.1 shows a mosaic of 313 tracks of Chang'E-1 imagery covering the whole lunar surface. To systematically investigate the FTTP problem on Chang'E-1 imagery, 26 tracks of Chang'E-1 images were selected from the 313 tracks and evenly distributed on the lunar surface. It should be noted that this study aims to produce a representative study of the FTTP problem on the lunar surface. The selected study areas cover the latitudes from -70° to 70° . The extreme cases in the pole regions are not included in this study. Figure 2.1 also illustrates the coverage of the 26 selected tracks of images.

For each image track, two individual operators, trained to be familiar with the FTTP problem, examined the entire image and marked the craters which displayed obvious

FTTP problems. Craters marked by both operators were identified as having FTTP problems in common. They are marked by white dots on Figure 2.2. It should be noted that, only those craters which are clearly recognizable (with a diameter larger than 5 km) on Chang'E-1 imagery are considered in this interpretation process. Through this progress, general situations of FTTP on lunar orbiter imagery could be obtained.

In Figure 2.2, a total of 210 craters were identified as having FTTP problems. The crater locations (latitude and longitude of the centre), diameters, and depths were then determined based on the crater topographic models. The crater topographic models were generated by using the Chang'E-1 stereo imagery and laser altimeter from LRO. The resolution for the crater topographic models is 360 m. Table 2.1 shows examples of the recorded detailed information of the identified craters and Table 2.2 summarizes the recorded information of craters with FTTP problem.

Table 2.1 Examples of the recorded information of craters with FTTP

Crater Series	Track Number	Latitude (N)	Longitude (E)	Diameter (km)
1	CE1_BMYK_CCD- B_SCI_N_20071121111841_20071121132623_0172_B	45.82	64.21	9.5
2	CE1_BMYK_CCD- B_SCI_N_20071121111841_20071121132623_0172_B	40.97	65.83	10.5
3	CE1_BMYK_CCD- B_SCI_N_20071121111841_20071121132623_0172_B	-56.65	67.07	7.5
4	CE1_BMYK_CCD- B_SCI_N_20071121111841_20071121132623_0172_B	-58.78	66.15	6.5
5	CE1_BMYK_CCD- B_SCI_N_20071121111841_20071121132623_0172_B	-53.31	67.02	6
6	CE1_BMYK_CCD- B_SCI_N_20071121111841_20071121132623_0172_B	-47.26	65.13	12
7	CE1_BMYK_CCD- B_SCI_N_20071122083550_20071122104333_0182_B	-63.75	52.7	6
...

Table 2.2 Summary of the craters with FTTP observed on Chang'E-1 imagery

Total crater numbers	210	
Crater diameter	Maximum	80 km
	Minimum	5 km
	Mean	15.76 km
Crater depth	Maximum	6 km
	Minimum	0.4 km
	Mean	2.18 km

Figure 2.3, 2.4 and 2.5 below show typical terrain objects with the FTTP problem. Figure 2.3 shows two distinct objects near the Apollo 15 landing site which are the rima called Rima Hadley (Figure 2.3 (b)) and the crater named Hadley C (Figure 2.3 (c)). Rima Hadley is a fake ridge within a circle of 80 km diameter. The diameter of the crater Hadley C is 5.5 km which belongs to the small size group among the craters identified with FTTP. Figure 2.4 shows an unnamed crater located in 53.48 N and 178.6 E, and with a diameter of 15 km which belongs to the median size class. The extra brightness of its surface makes it different from others. The large crater named Aristillus in Figure 2.5 has a diameter of 50 km. The group of apexes which appear as cavities in its centre make it obvious.

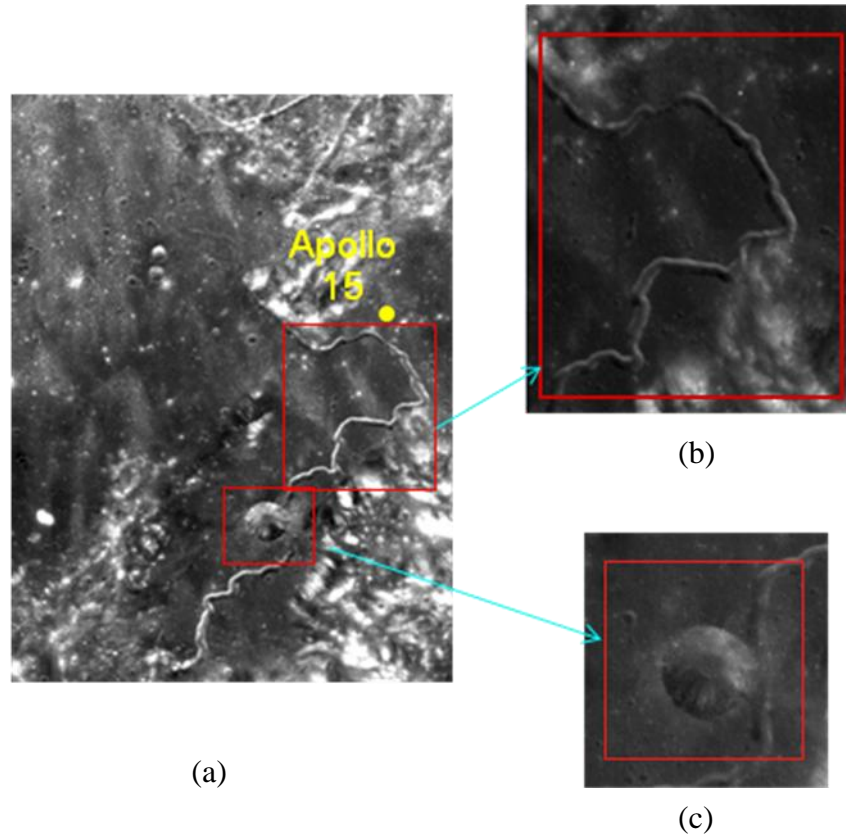


Figure 2.3 Example of FTTP. a) Apollo 15 landing site area, b) Rima Hadley, and c) Hadley C



Figure 2.4 A typical crater with median size

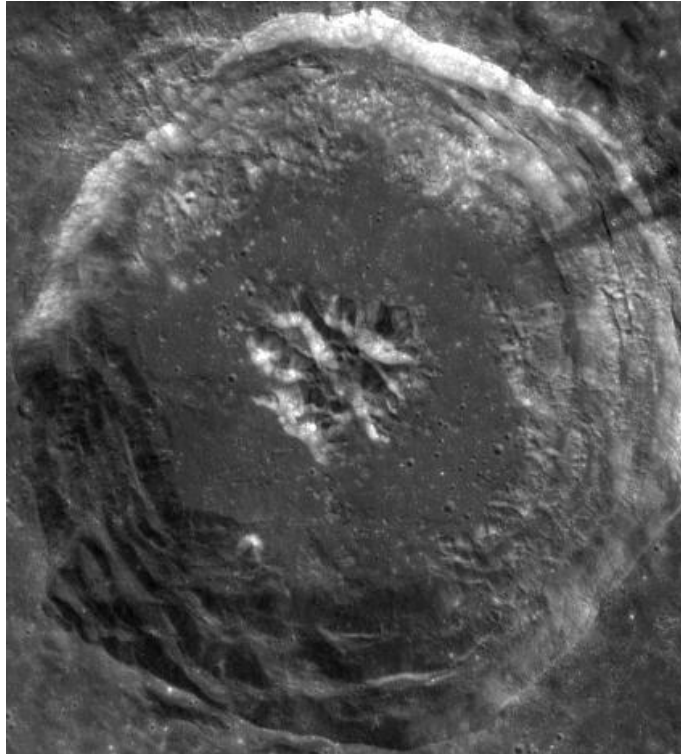


Figure 2.5 Aristillus crater

2.2 Analysis of Factors Related to FPHP Problems

2.2.1 Relationship between FPHP and Object Locations

To analysis relationship between FPHP and locations of craters, two histograms have been generated separately (Figure 2.6 and Figure 2.7).

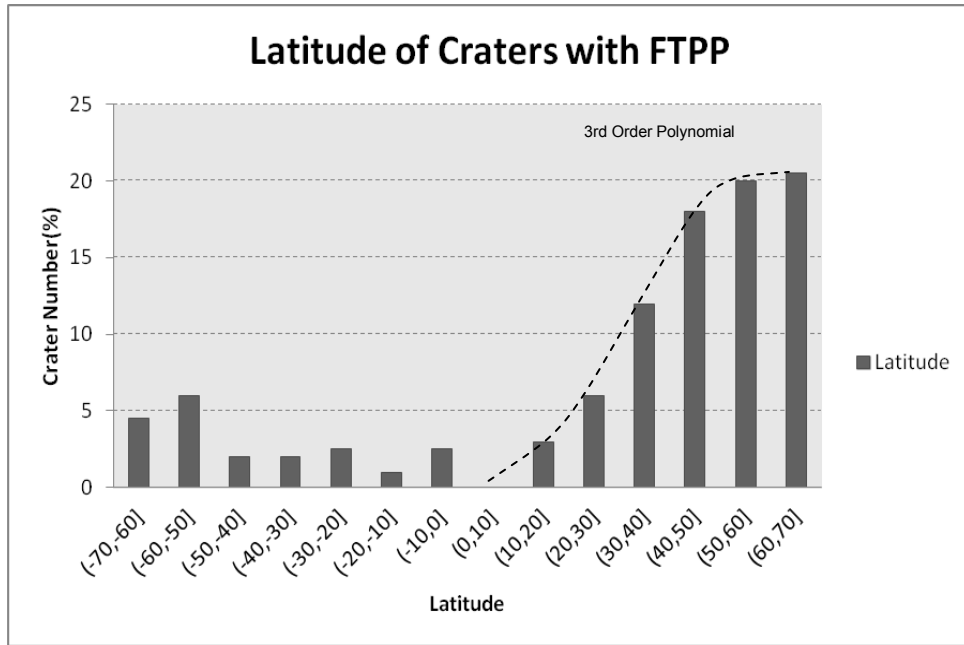


Figure 2.6 Histograms of craters suffering from FТП with latitude

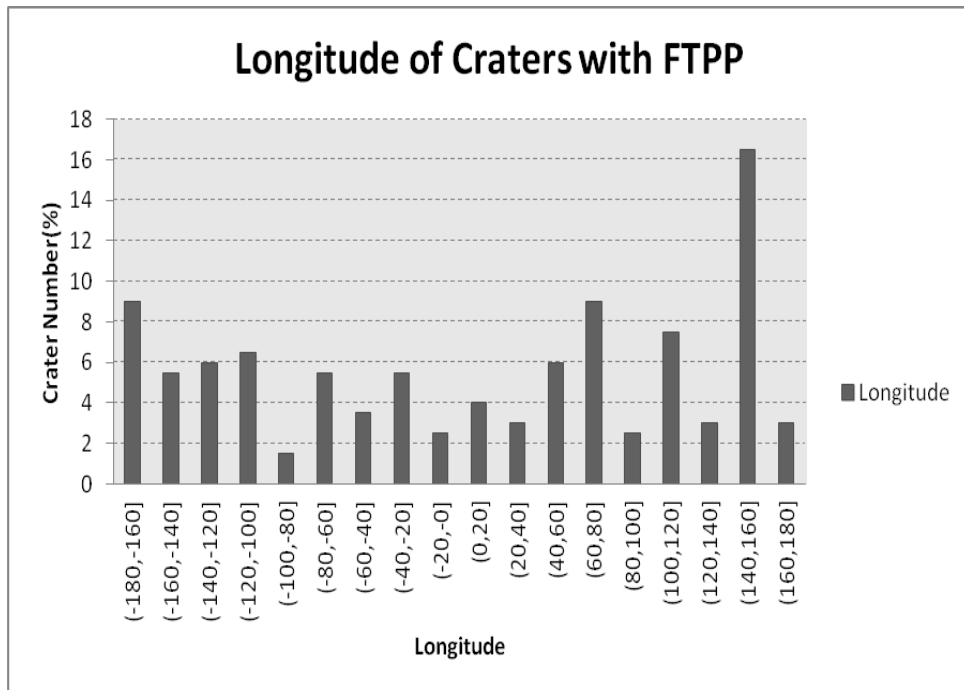


Figure 2.7 Histograms of craters suffering from FТП with longitude

In Figure 2.6, it is clearly seen that FTTP problem in the north hemisphere is much more serious than that of the south. The north pole region suffers from extremely serious FTTP problems, a feature also been reported by Saraf et al. (2011).. The FTTP trend of FTTP is almost increasing progressively from the equator to the poles in the northern hemisphere. The relationships can be generally modelled by a third-order polynomial as illustrated in Figure 2.6.

Two reasons may relate to this characteristic. The first one is as follows: by looking at the lunar map as shown in Figure 2.2, the equator areas are flatter and smoother than the areas close to the poles. FTTP could not be occurred in the plain, thus equator gives the least FTTP data and also for the surrounding areas. The second reason is about the illumination directions which can be used to explain the significant unbalanced distribution of craters with FTTP between the two hemispheres as indicated in Figure 2.2. The Moon and Earth have the similar sun illumination conditions. Of these conditions the perpendicular incidence of sun will shift within 1.6 degrees lines of two hemispheres while 23.5 degrees in the earth. In addition, data used in this investigation were mainly taken from December 2007 to January 2008. Thus the north part below 1.6 degrees south latitude in south hemisphere and the whole north hemisphere will always have the illumination comes from south while south part of 1.6 degrees south latitude will always receive the sunlight from north. Referring to the assumption of light-from-above in human visual perception as discussed previously, the north part above 1.6 degrees south

latitude has more chance to suffer FPHP. It can be concluded that the FPHP is positively correlated to the latitude in the north part of 1.6 degrees south hemisphere for it will always get the illumination from south. From the observation in this study, the North Pole region suffers from extremely serious FPHP problems, a feature also been reported by Saraf et al. (2011).

As for the craters identified with FPHP in the southern hemisphere, this could be explained by the following two reasons. Firstly, the specific characteristics of some craters and the related illumination conditions on the images may affect the perception of the operator. For example, some crater may be perceived as hillock due to the relatively large protrusions inside the crater, and some large shallow crater might be perceived as pop-out when there is no much difference between the illumination condition of the crater and its nearby region. Secondly, the psychological process of the operator may influence the perception. When the operators examining each strip of the Chang'E-1 images from bottom (south) to top (north), it is more likely for them to identify craters with FPHP since they are undergoing a psychological process from light to heavy FPHP situations and the comparison of craters in local regions may lead to deviated perceptions

The craters with FPHP problems along the longitude direction are more evenly distributed as shown in Figure 2.7. Therefore, it can be concluded that the FPHP is not related to the longitude.

2.2.2 Relationship between FTTP and Crater Shapes

Crater shape is another important factor related to FTTP. The ratio I (d/D) of rim-to-floor depth (d) to the rim-to-rim diameter (D) has been widely used in the past to characterize the crater shapes on the Moon and Mars (Moutsoulas and Preka, 1981; Stepinski, 2010). The smaller the I , the flatter the crater. This study also employed the ratio I of crater in the analysis of the relationship between FTTP and crater shapes.

The FTTP situations of the craters were classified into five different levels (5, 6, 7, 8, 9) based on the serious of FTTP degrees, with 5 representing light FTTP and 9 representing heavy FTTP. Two individual operators examined all the pre-identified 210 craters and classified them into different levels. It should be noted that those craters, classified by the two operators as having inconsistent FTTP levels were excluded from this study. Table 2.3 below shows the sample of data collection. Finally, 70 craters located in a relatively narrow range of latitudes (from latitudes 50° to 65°) were selected for the sake of similar sun illumination conditions.

Table 2.3 Sample of data collection

Crater ID	depth(d)/km	diameter(D)/km	$I=d/D$	FTTP Levels
1	3.5	32	0.109	9
2	3	33	0.091	7
3	6	48	0.125	7

3	5	15	0.333	8
4	0.8	52	0.015	6
5	2	10	0.2	8
6	1	15	0.067	7
7	1.5	8.5	0.176	8
8	4	43.5	0.092	7
9	2.5	9	0.278	8
10	1	14.5	0.069	8
11	1	15.5	0.065	8
12	2.5	30	0.083	7
13	2	15	0.133	8
14	2	11	0.182	8
15	2	14.5	0.138	8
...

Figure 2.8 and Figure 2.9 show the histograms of the craters in this analysis. Figure 2.8 shows the crater distributions with respect to different FTTP levels. From this histogram, it can be seen that most of the craters suffer from serious FTTP problems as indicated in the level 8 and 9 columns. Level 8 contains 33 craters as the biggest group. Figure 2.9 gives a histogram showing the distribution of craters with respect to different ranges of crater shape ratio I . The ranges are determined based on a classification process of the shape ratio values of all craters. Within each range, the FTTP levels are illustrated using different grey scales. Darker colours represent more serious FTTP problems. In Figure 2.9, it can be seen that most of the craters have ratio values between 0.11 and 0.21, and that colours strengthen from left

column to right, indicating FTPP degrees are heavier for craters with larger depth-diameter ratio values.

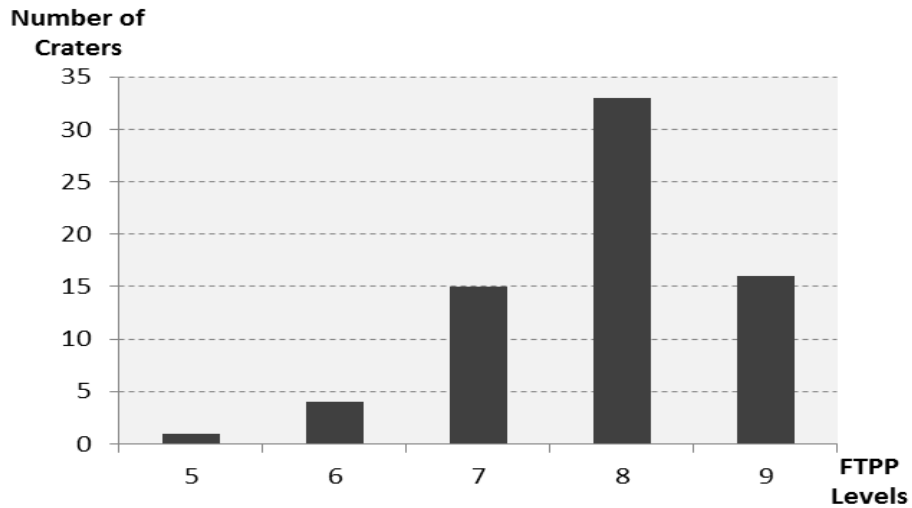


Figure 2.8 Histograms of the craters with respect to different FTPP levels

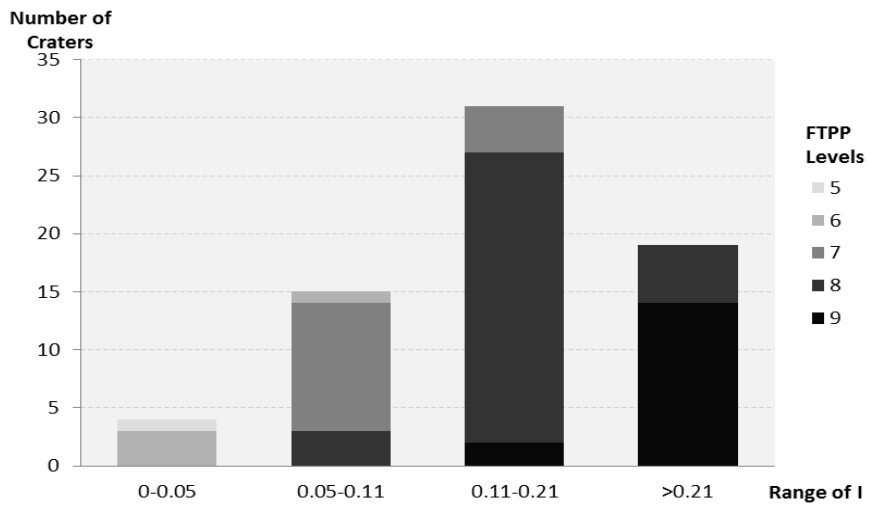


Figure 2.9 Histograms of the craters with respect to different ranges of crater shape ratio I

To further study the FTPP level distribution pattern as regards the crater shapes, two more charts were generated as shown in Figure 2.10 and Figure 2.11. Figure 2.10 shows the distribution of FTPP levels with respect to crater shapes for all the craters. It can be seen that FTPP is lighter, in general, for craters with smaller depth-diameter ratio values. To analyse the distribution pattern more generally, the RMS value of the shape ratio I were derived for each FTPP level and were plotted and shown in Figure 2.11. The distribution trend shown in Figure 2.11 indicates that FTPP levels increase in line with the depth-diameter ratio I . This suggests that the deeper and smaller craters have heavier FTPP problems than the flatter and larger ones. The FTPP level distribution trend regarding the average depth-diameter ratio can be modelled by a second-order polynomial as illustrated in Figure 2.11.

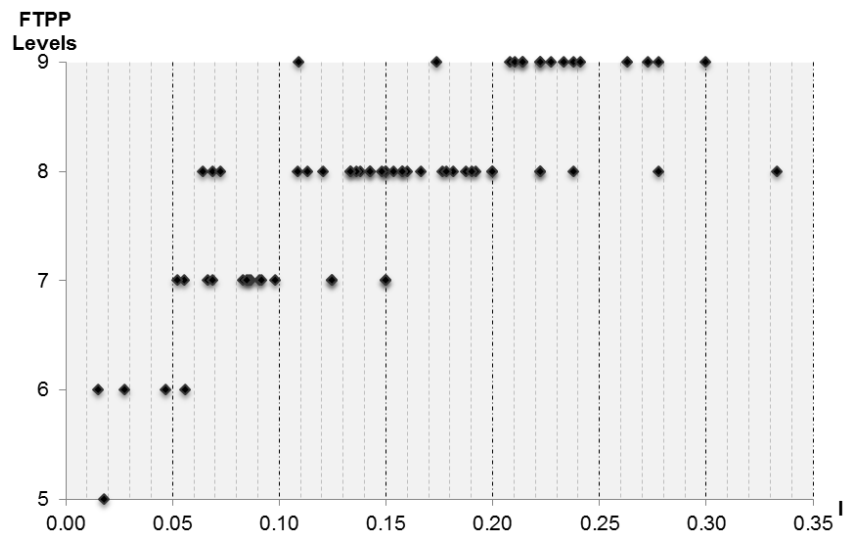


Figure 2.10 Distribution of FTPP levels with respect to crater shapes of all examined craters

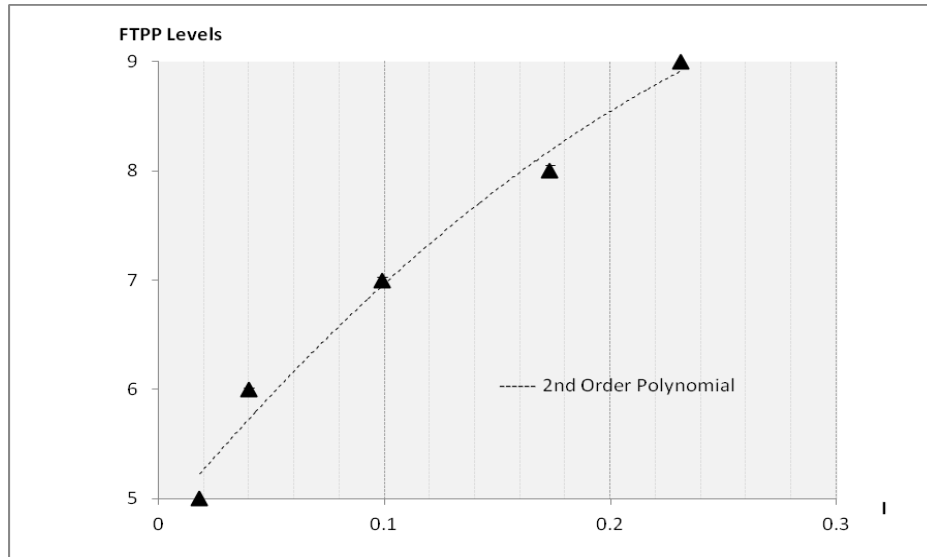


Figure 2.11 Distribution of FTPP levels with respect to crater shapes with RMS of I in each FTPP level

2.2.3 Other Factors Related to FTPP

Azimuth angle of the illumination direction is the most important factor leading to the development of FTPP. Azimuth angle is defined as the angle between the sun incident direction and the true north which is a representation of illumination direction. Light coming from the south will lead to FTPP while the azimuth angle in this case is within the range from 90° to 270° . To investigate the influence of the illumination azimuth angle on FTPP within this range, craters suffering from FTPP and having different illumination azimuth angles were examined. Figure 2.12 shows a typical example observed in Chang'E-1 images. Figures 2.12 (a) and (b) are the same crater, but with different illumination azimuth. Figure 2.12 (a) has an angle of

160° and the one in Figure 2.12 (b) has an angle of 260°. From Figures 2.12 (a) and (b) it can be seen that different illumination azimuth angles make the crater shape look different, while the FTTP problem occurred in both situations, the levels of which are similar.

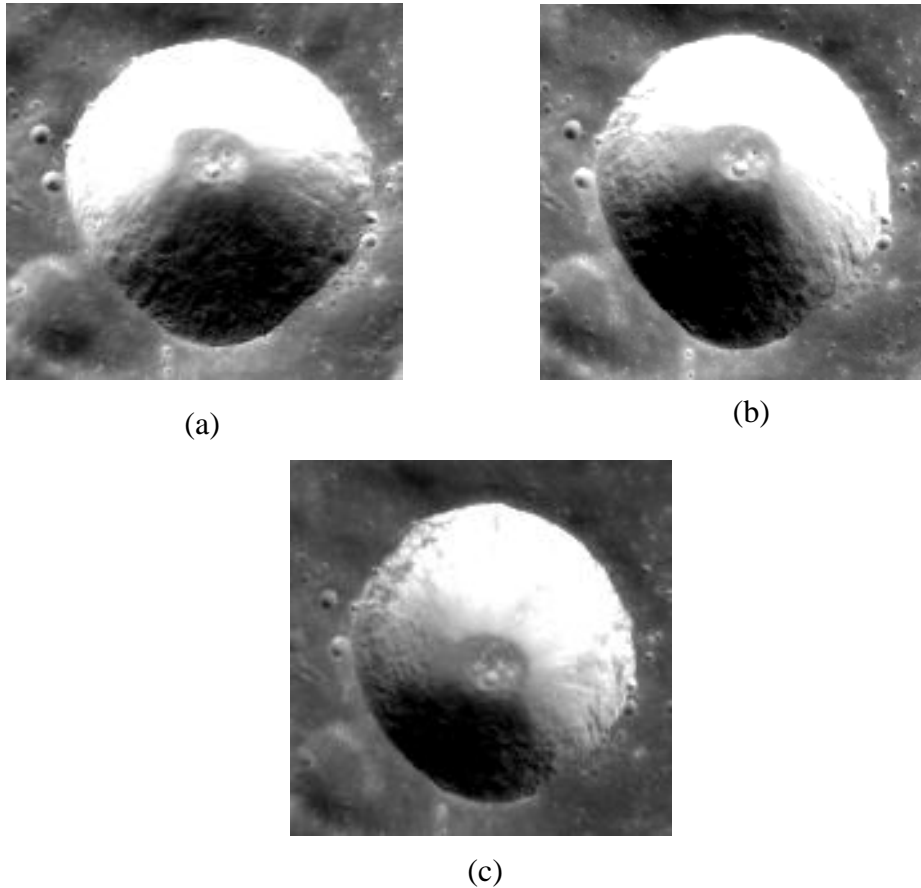


Figure 2.12 A crater at different illumination azimuth angles and viewing angles: (a) shows a 160° azimuth angle and -16.7° viewing angle, (b) a 260° azimuth angle and -16.7° viewing angle, and (c) a 260° azimuth angle and a 16.7° viewing angle

The viewing angle could slightly affect the FTTP because the shadow and shape of

the crater could vary from different viewing angles. Figure 2.12 (c) shows the same crater in Figure 2.12 (b) while has a different viewing angle. The crater shown in Figure 2.12 (c) has a viewing angle of 16.7° (forward looking), while that in Figure 2.12 (b) has a view angle of -16.7° (backward looking). From the observations and experiments in this study, it has been found that the viewing angle is not a significant factor influencing the FTTP.

The Sun elevation angle is another important factor to affecting FTTP. Smaller elevation angle will cause larger shadow areas in the satellite image, which, in consequence will lead to more serious FTTP problems. The formula of sun elevation is " $h=90^\circ-|\varphi-\delta|$ ", which h stands for the sun elevation, φ is the local latitude and δ is the current Sun declination. According to this formula, sun elevation decreases in line with the increasing of latitude. Thus the object in pole district has lower sun elevation and stronger shadow. Therefore, high latitude areas in the northern hemisphere of the Moon suffer from heavier FTTP problems compared with those of the equator areas, a factor which has been statistically verified above in section 2.2.1.

To simulate various sun elevation angles of the same objects, two sets of DEMs with different depth-diameter ratios were selected to generate Shaded Relief Maps (SRMs). The azimuth angles were fixed in 225 degrees to obtain the strongest FTTP effect, and seven sun elevations were chosen from 0 to 90 degrees with an equal

interval of 15 degrees. Figure 2.13 and 2.14 show these two sets SRMs in different elevation angles.

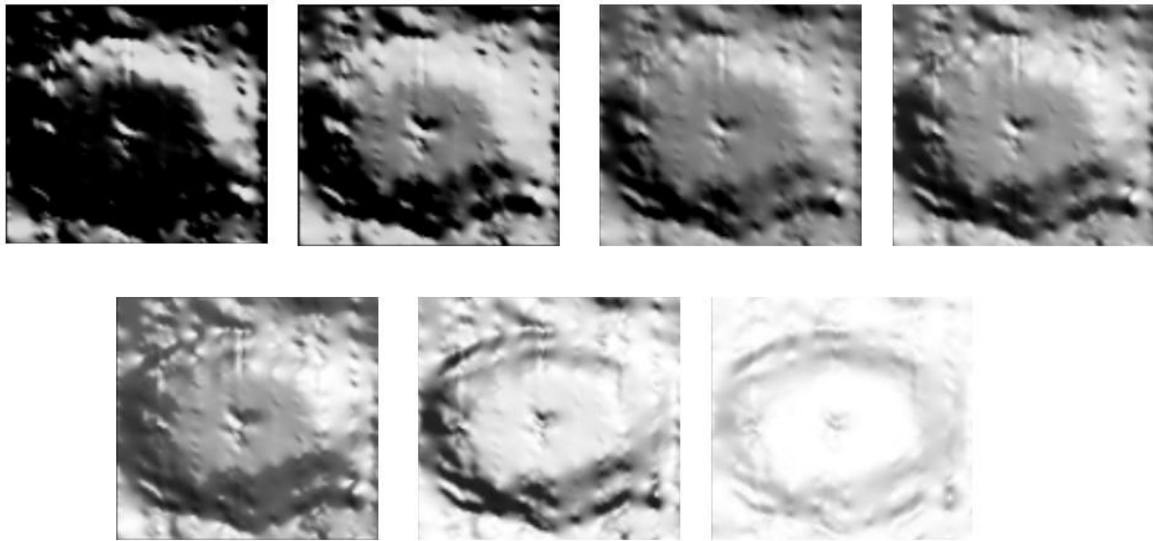


Figure 2.13 SRMs of a median size crater with azimuth angle of 225 degrees and sun elevation angle of: a) 0 degree, b) 15 degrees, c) 30 degrees, d) 45 degrees, e) 60 degrees, f) 75 degrees, and g) 90 degrees.

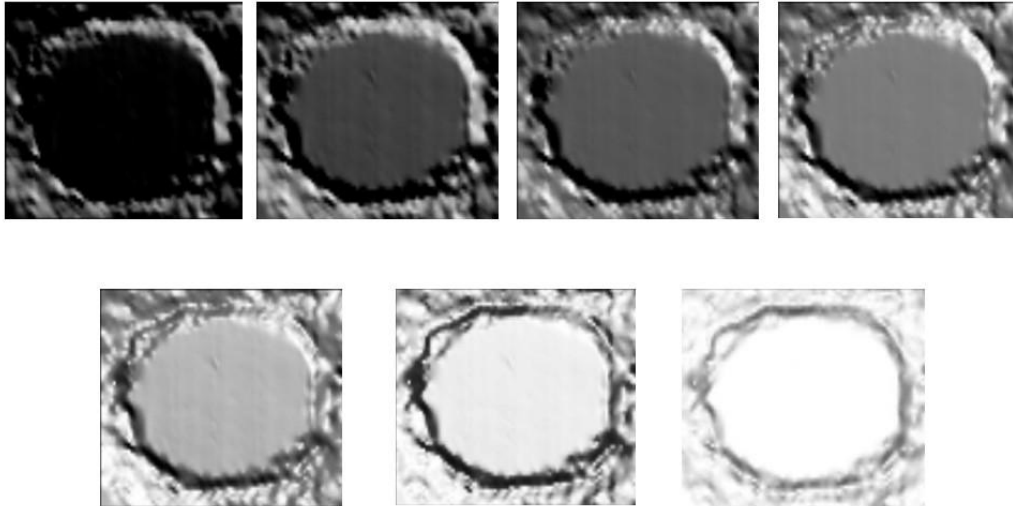


Figure 2.14 SRMs of a large size crater with azimuth angle of 225 degrees and sun elevation angle of a) 0 degree, b) 15 degrees, c) 30 degrees, d) 45 degrees, e) 60 degrees, f) 75 degrees, g) 90 degrees.

Through Figure 2.13 and 2.14, of the same azimuth angle, the effect of sun elevation angle depends on shape value I . Though the huge shadow in 0 degree gives a similar impression of concave, the effects become different at 15 degrees. The crater in Figure 2.14 (b) has smaller depth-diameter ratio than that show in Figure 2.13 (b), and the FTTP level of Figure 2.13 (b) is more serious (more like an apex) than that of depicted in Figure 2.14 (b). The FTTP levels are all getting serious from 15 degrees to 75 degrees. Then they all turn to flat under the vertical elevation angle. This is because under the direct illumination of the sun, the area becomes too bright to show the details. Images without shadow lead to the problem of perception depth. It can be generally concluded that the FTTP levels are more serious with the increase of the sun elevation angle.

Chapter 3 Remediation of FTPP on Lunar Imagery

This chapter mainly discussed the methods to alleviate the FTPP problem on lunar orbiter imagery, which include traditional methods such as image rotation and DN reversion and two novel methods such as a wavelet-transform based approach and a rotation invariant approach.

3.1 Traditional Methods

3.1.1 Image Rotation

Rotating the image by 180 degrees is the most traditional method to solve FTPP, and it is the simplest way for FTPP treatment (Saraf et al., 1996).

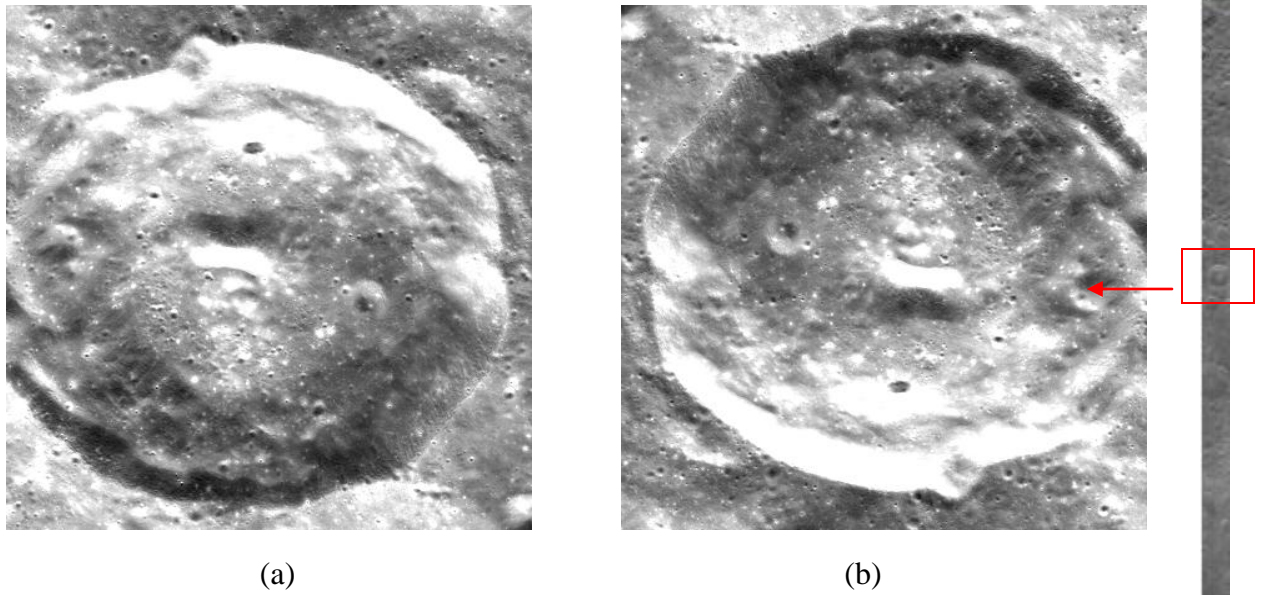


Figure 3.1 (a) A crater in Chang'E-1 image track 0435, (b) FTPP-corrected by rotation

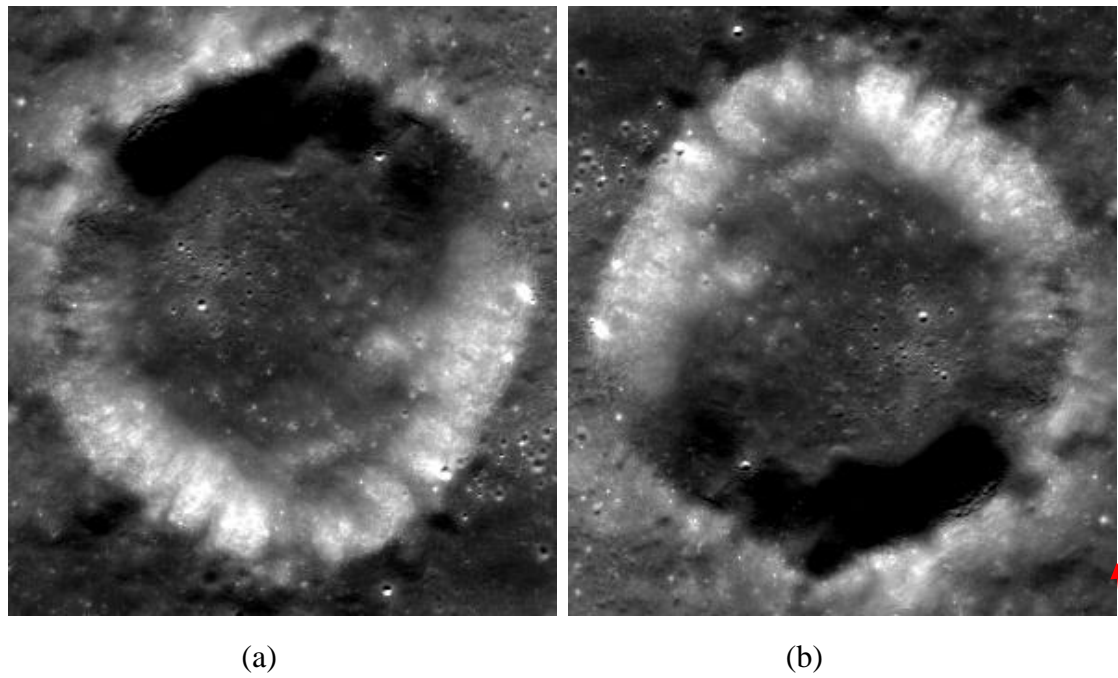


Figure 3.2 (a) A crater without FTPP also in track 0435, (b) the rotated image which suffers from the FTPP

Figure 3.1 shows an example of using image rotation to correct the FTTP problem. As it represents, image rotation works for a single crater. But when rotating the whole image track, the other parts of the images get affected, see Figure 3.2. The crater in Figure 3.2 (a) comes from the same track of image with the crater in Figure 3.1 (a). It does not effect from the FTTP through observation. By doing image rotation, the crater in Figure 3.2 (a) changed to the FTTP suffering one (Figure 3.2 (b)). As it is hard to separate the objects with the FTTP problem and FTTP unaffected ones before rotation, all the objects in the image were rotated at once. By applied this method to lunar imagery, the FTTP in north hemisphere could be eliminated while it appears in south hemisphere. Thus image rotation might be not a suitable solution for the lunar data set.

Image rotation could not correct any FTTP effectively. As shown in Figure 3.3, compared Figure 3.3s (a) and (b), image rotation gave a weak impact for the FTTP alleviation, as the two craters in Figure 3.3 both represented as apexes. This can also be found in Figures 3.4 (a) and (c), which we could clearly define it as FTTP by its enlarged image in Google Moon (Figure 3.4 (b)). In enlarged image using Google Moon (Figure 3.4 (b)), the objects seemed as a valley while it appeared as ridge both in Figures 3.4 (a) and (c). Thus the rotation approach did not work for the rima in Figures 3.4 (a). There are several reasons to explain why image rotation does not work in these cases. The limitation of resolution is one of the reasons. The size of this crater and limited resolution cause the lack of details. Weak illumination makes

this situation even worse. For above reason, it is hard to identify the boundary of light part and shadows. Thus the reliefs are weak in both FTTP image and the corrected one.

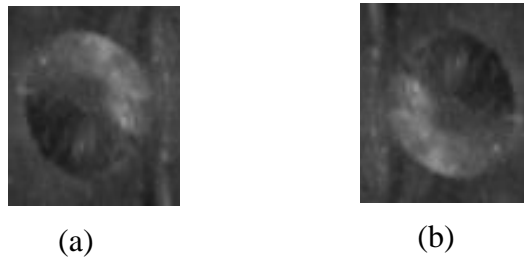


Figure 3.3 (a) Hadley C, (b) Rotated Hadley C

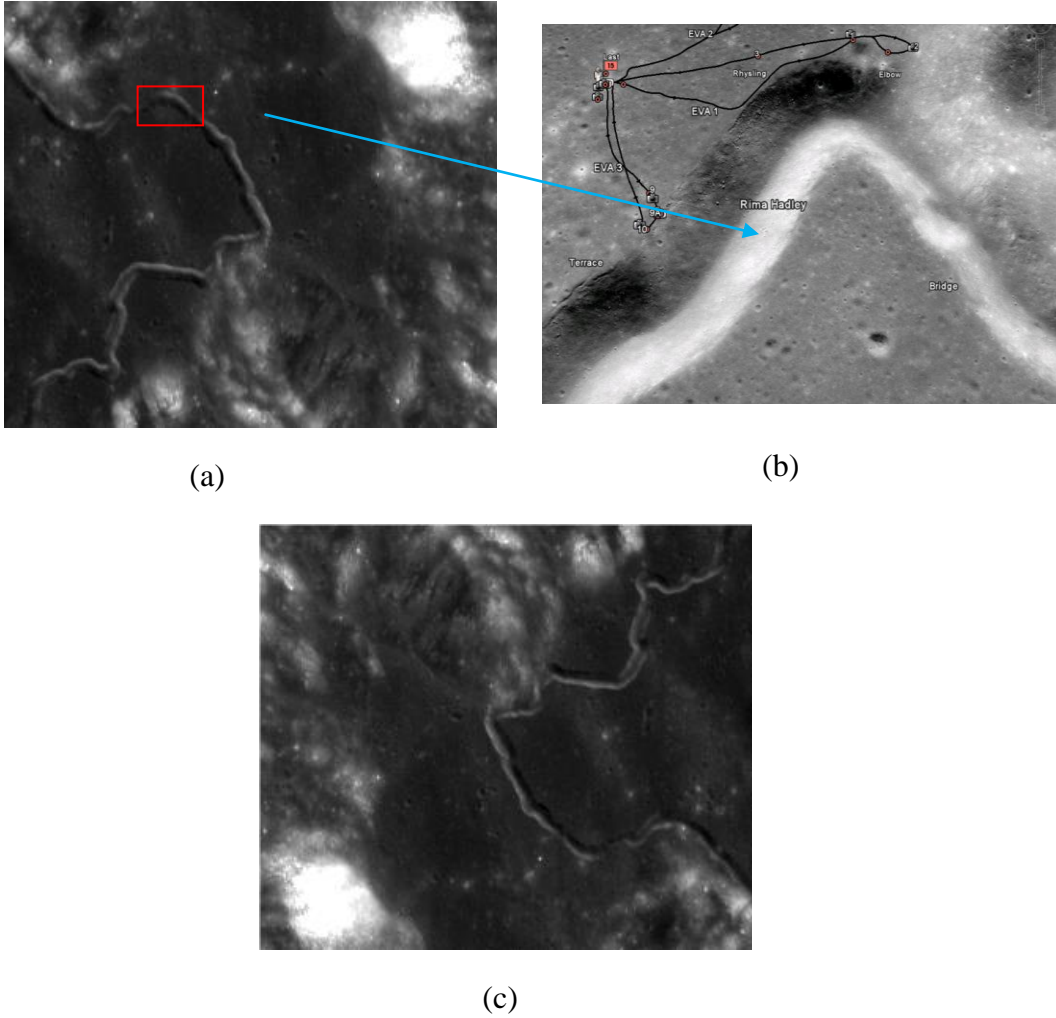


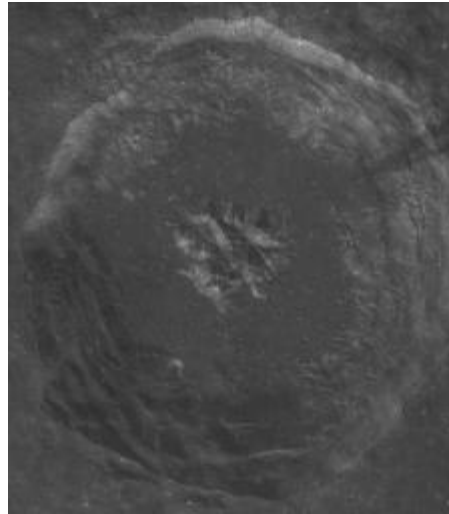
Figure 3.4 (a) Part of Rima Hadley, (b) Enlarged View by Google Moon,
(c) Rotated Rima Hadley

Another drawback for image rotation is that it makes the north direction appear in the bottom which is inverted from the common cartographic way. Thus sometimes the rotated image resembles a completely new one and the topology of objectives changed as well. This brings new problems in image perception.

3.1.2 Digital Number Value Inversion

The Digital Number value inversion method uses DN (digital number) values to do the inversion, which subtracts the grey value of each pixel from 255.

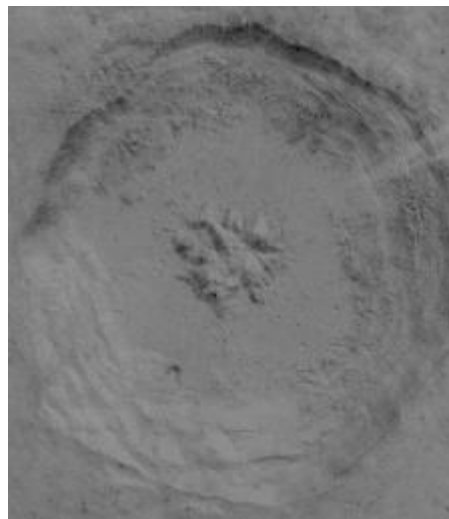
Figure 3.5 (a) and (b) show a comparison between FTTP crater and the FTTP free one using the original “subtract from 255” DN inverted method. By comparison, the former one looked like an apex and the Figure 3.5 (b) seemed as a crater. Thus the method is worked in this case, but the image is obviously over lighting, for it is too white .A lot of details lost in the transformation. To reduce the illumination, the “255” Digital Number value in the original formula need a deduction. To find a suitable value, we need to examine the DN value table of the image. As in a range of 0 to 255, DN value usually gets the max value smaller than 255. It is 195 in this example. Replacing 255 by 195, Figure 3.5 (c) gives the resulting image. Obviously this image is clearer than the image in Figure 3.5 (b), but still it is difficult to see the land cover details. Figure 3.5 (d) is the final image after a further contrast enhancement through a de-quantized adjustment process. It is clear to see the topographic details including the unique apexes in the centre.



(a)



(b)



(c)



(d)

Figure 3.5 (a) Original crater Aristillus with FTTP, (b) Image after traditional DN Inverted method, (c) Image using advanced DN inverted method, (d) Final image free of FTTP

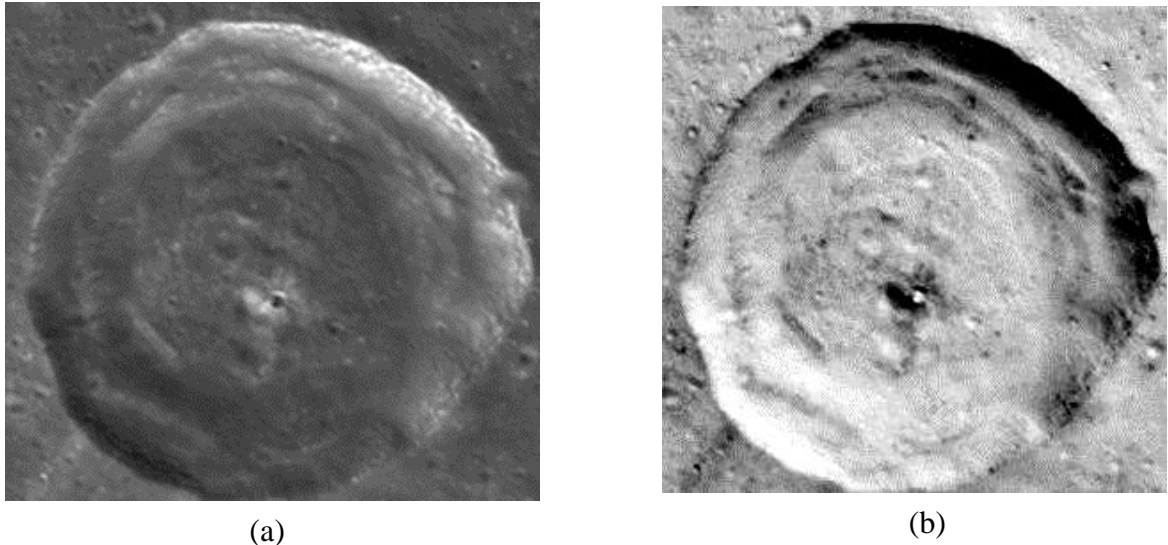


Figure 3.6 (a) Original image of a crater, (b) Resulting image after DN inverted

Another experiment was performed for the crater shown in Figure 1.1 (a), which will be further investigated in the following experiments. As shown in figure 3.6 (b), the resulting image was not quite satisfactory. Although the result has changed the illumination to the northeast direction successfully, the less shadow in north east and stronger light reflection in south west still made the crater like an apex. This is probably causing by the poor illumination condition of the original imagery. The textures of the image have also been changed significantly. Similar situations are common in the lunar imagery. Thus using DN reversion approach to eliminate the FTTP problem on whole lunar imagery could not be an appropriate choice.

3.2 A Wavelet-transform Based Approach for FTPP Remediation on Lunar Imagery

The main procedure of this method is to use DEM to simulate a proper illumination situation, and fuse those various illumination DEMs with original satellite images to obtain the FTPP-alleviated images.

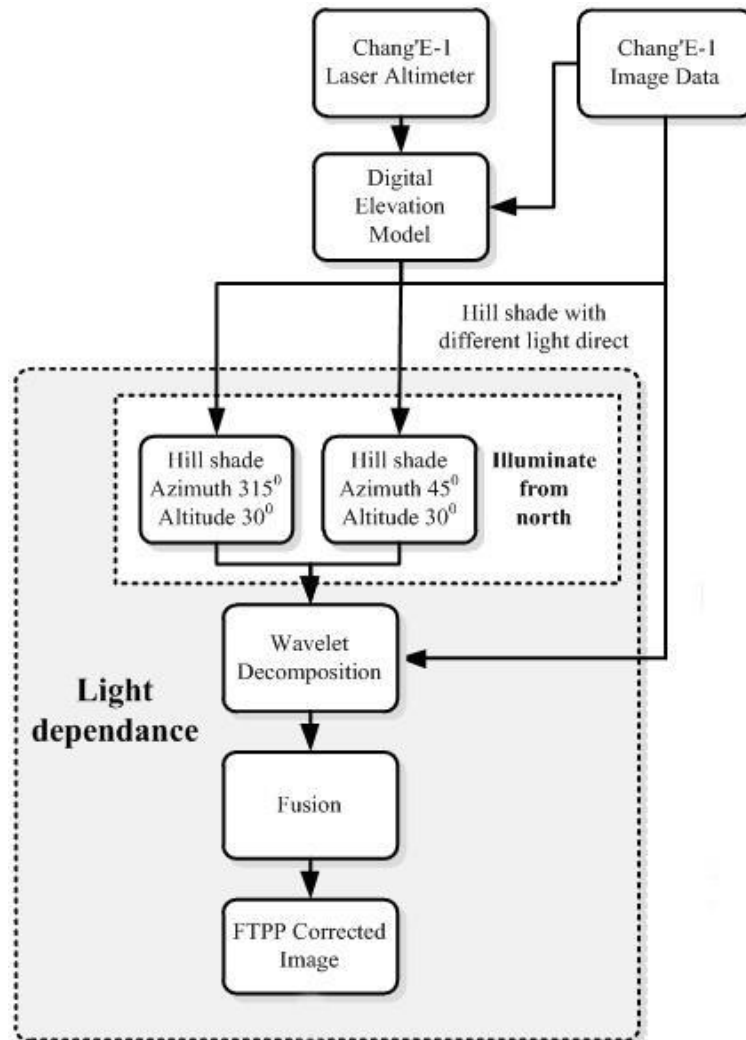


Figure 3.7 Overview of the wavelet-transform based approach

In this method, a high precision DEM is first generated using the Chang'E-1 images. Then shaded relief model is calculated via north light illumination, i.e. azimuth 315° and azimuth 45° . Finally, the SRMs with north light illumination used as reference images are fused with original images. A wavelet based image fusion method is employed to keep the features of both images.

3.2.1 Digital Elevation Model (DEM) and SRM Generation

(1) Photogrammetric Techniques for DEM Generation

A high precision crater DEM with a reasonable resolution is important for this method since it is the main contributor to correct the FTTP problem. If the precision of the DEM is low, distortions on the original image will be created during the image fusion. If the resolution of the DEM is distant from the image resolution, the performance of the FTTP correction will then be poor. In this study, the DEMs of craters were generated by using the Chang'E-1 stereo imagery and laser altimeter data through an integrated photogrammetric method. The resolution of the DEM is 360 m, which is three times of the resolution of the Chang'E-1 imagery (120 m/pixel) and is good for FTTP correction. The Leica Photogrammetry Suit (LPS) was used to obtain the DEM data. The detailed procedures for deviation of crater DEMs are described below.

Step 1: Select control points from the Chang'E-1 laser altimeter data.

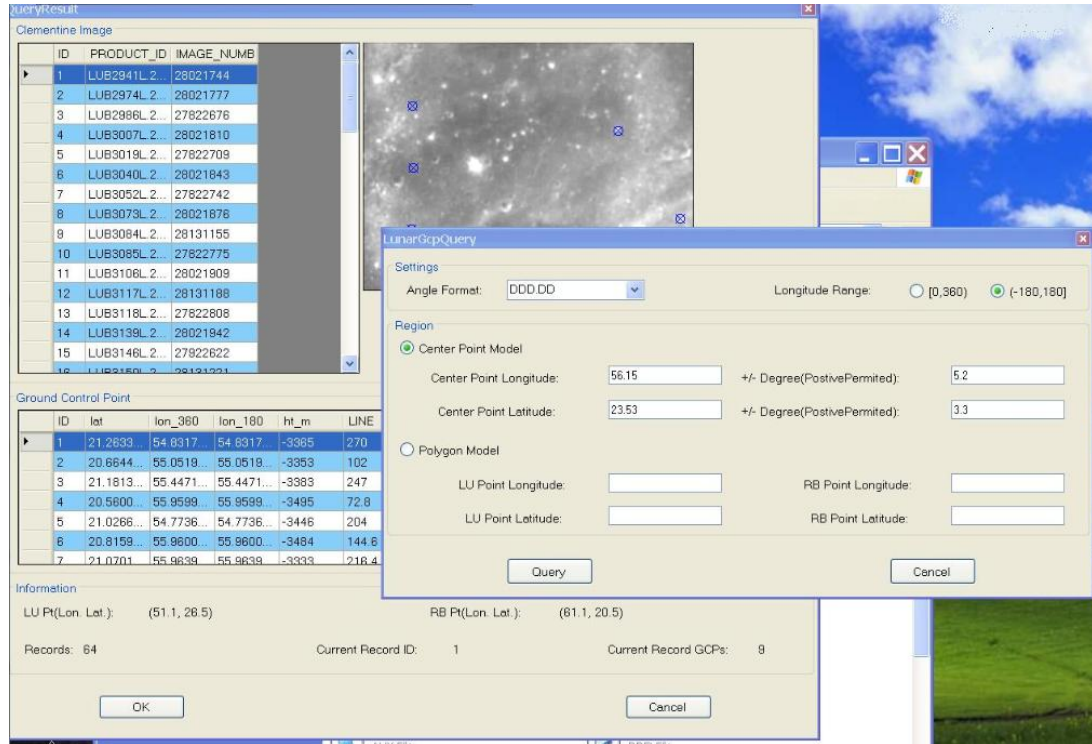


Figure 3.8 Interface of control points selection

Step 2: Set up software parameters according to the parameters of Chang'E-1 satellite.

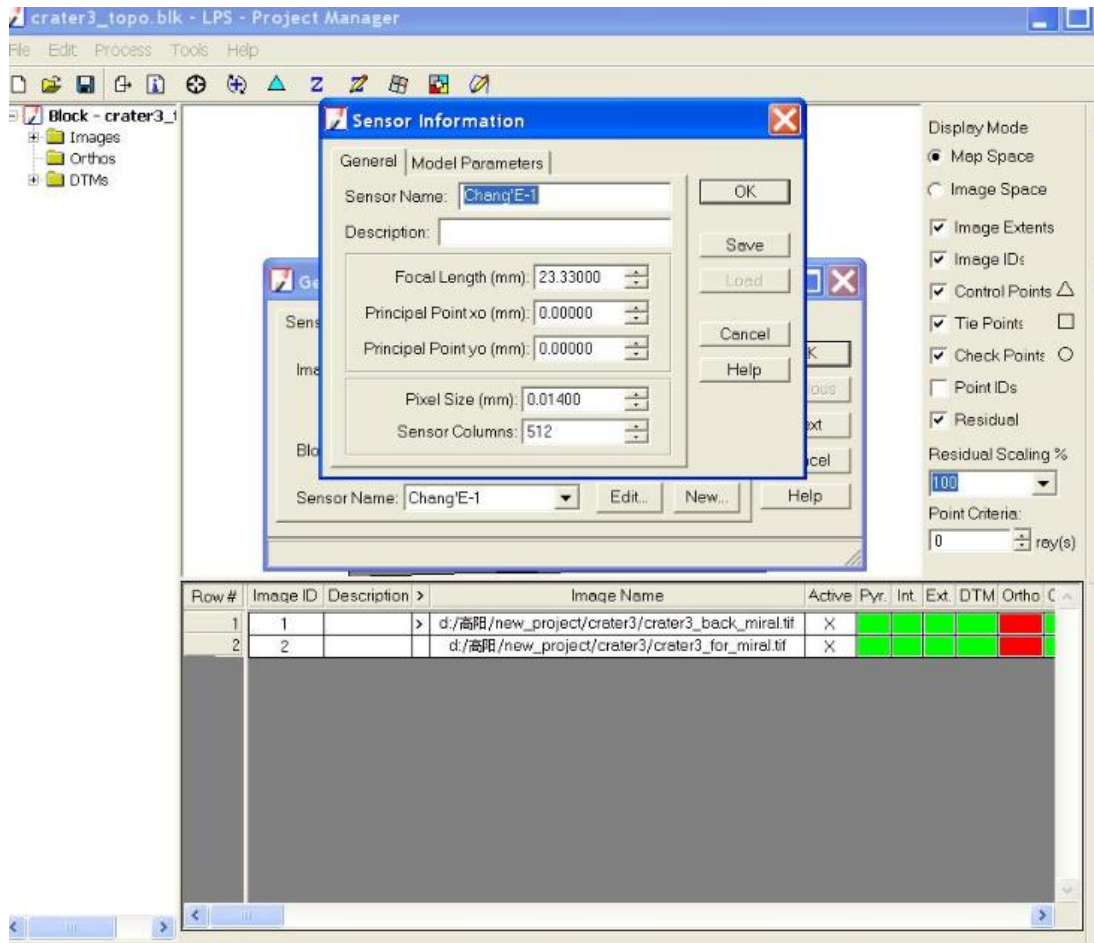


Figure 3.9 Interface of parameter setting

Step 3: Digitize the control points on both forward and backward images, and produce tie points for DEM generation.

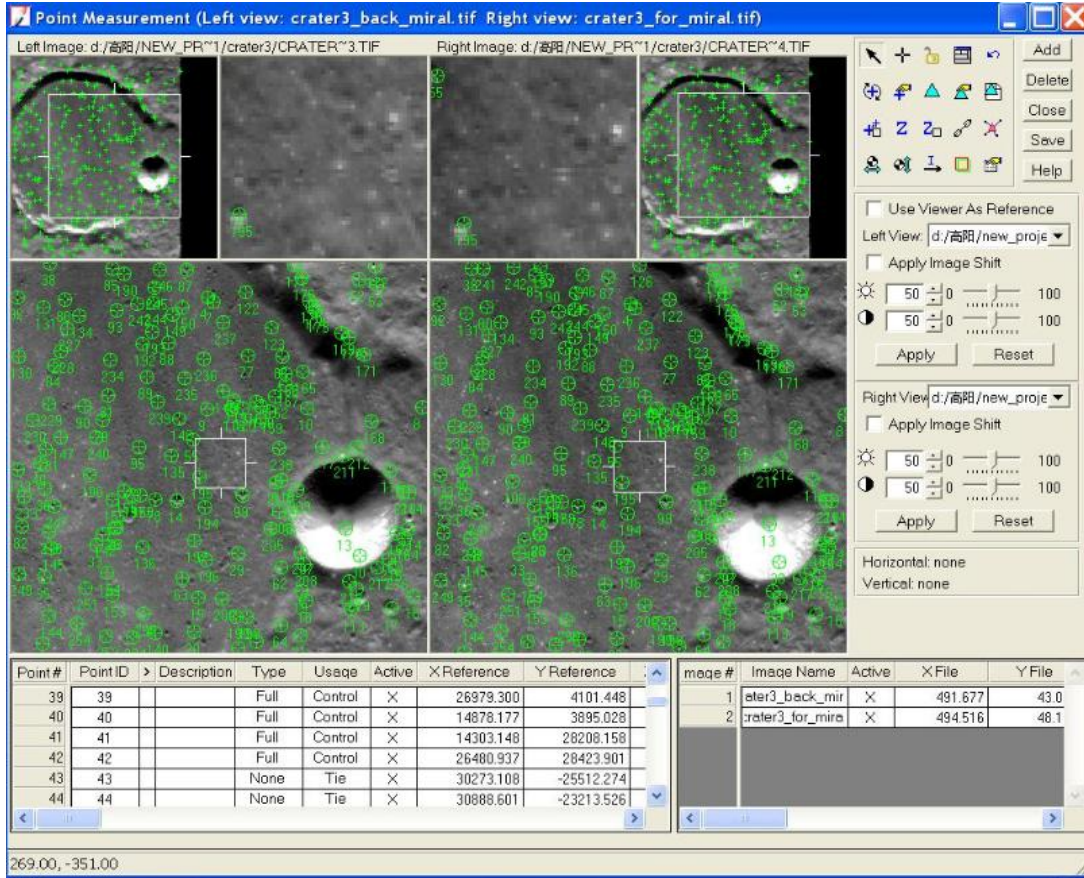


Figure 3.10 Interface of control points and tie points generation

Step 4: Extract the DEM and generate the Shadowed Relief Model (SRM).

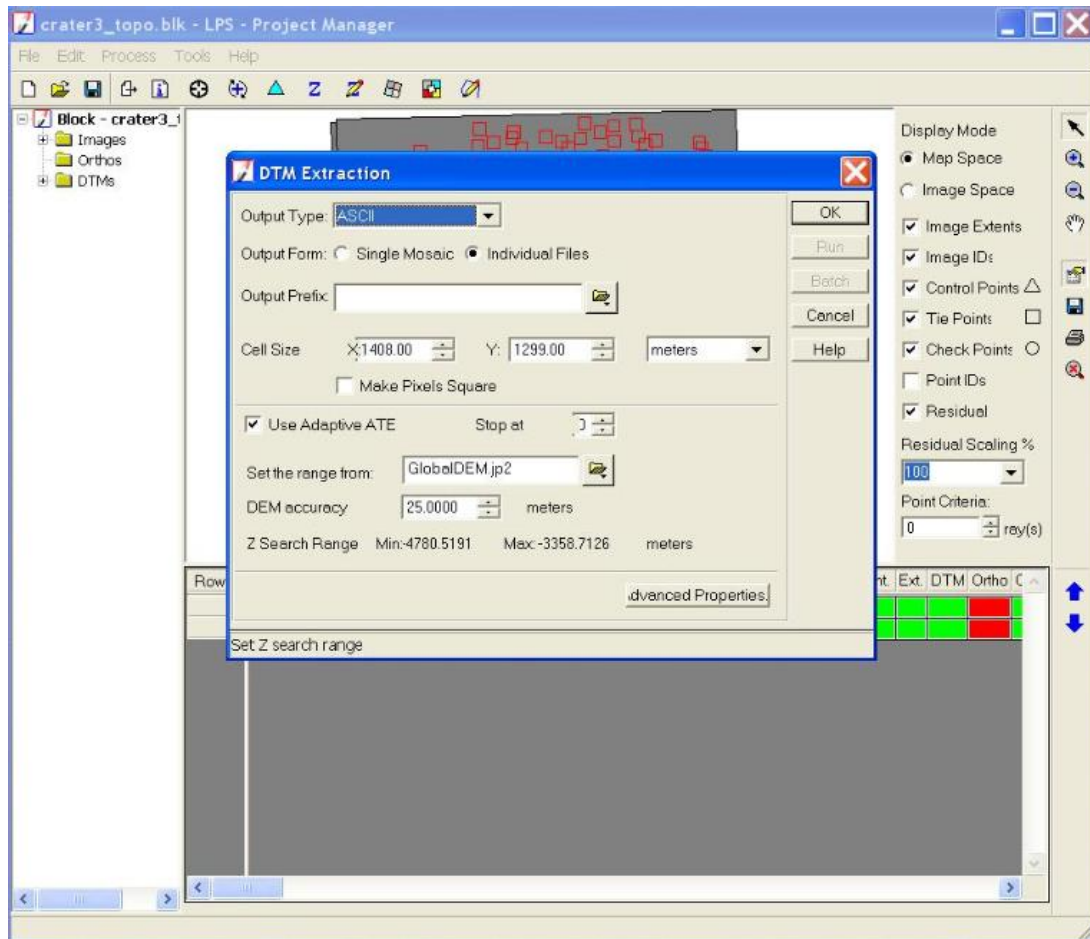


Figure 3.11 Interface of DEM extraction

Figure 3.12 shows the 3D views of the generated DEM of the crater (named as crater 1) shown in Figure 1.1 (a). This crater is located in (51.20 N, 43.60 E) with a diameter of 33 km and depth of 3 km.

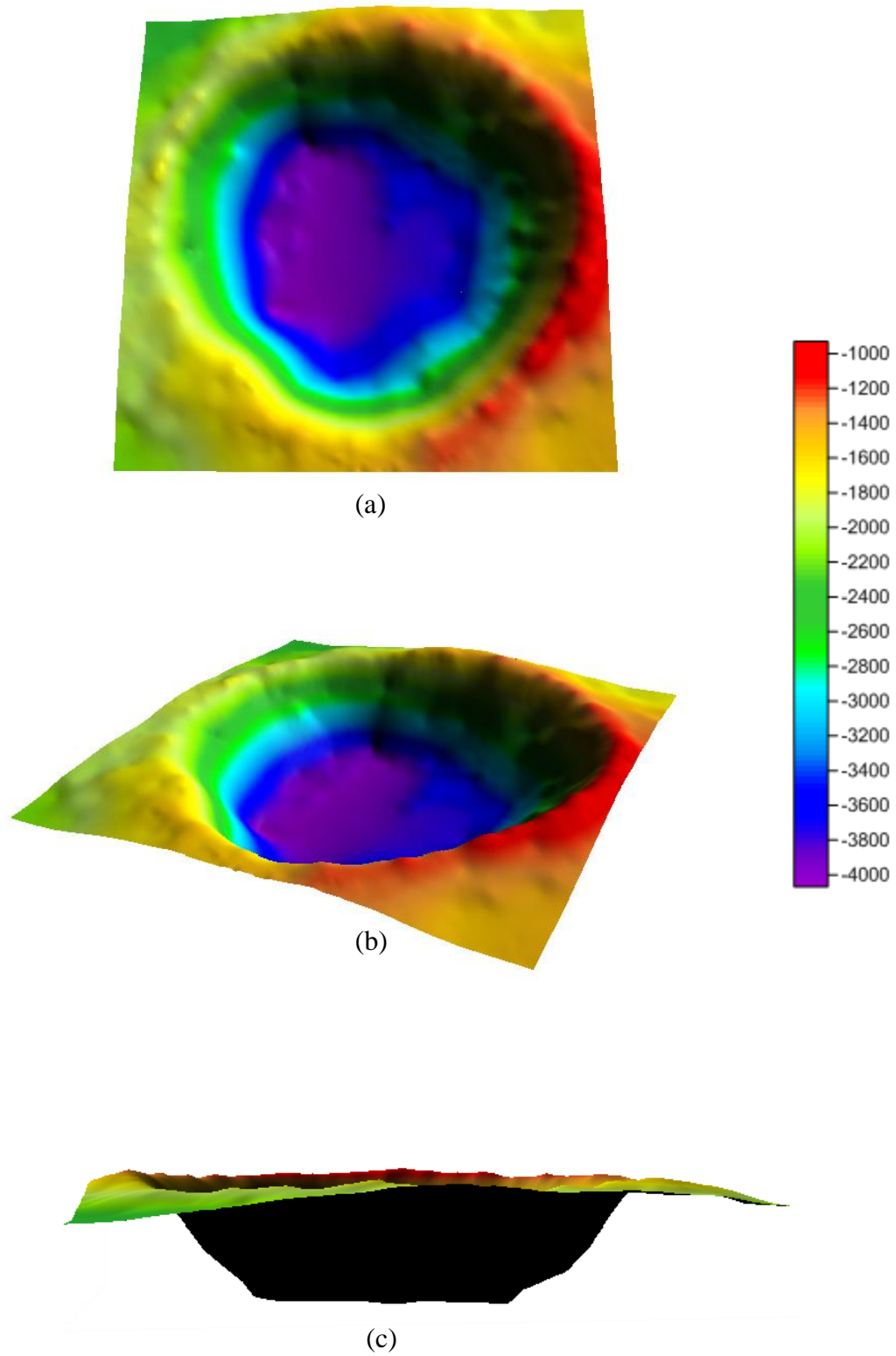


Figure 3.12 DEMs of Crater 1: (a) overhead view, (b) side view, (c) horizontal view

(2) SRMs Generation

According to the light-from-above prior, a reference image should be using north direction illumination to generate SRMs. In this generalization, we defined north azimuth equal to 315 degrees and 45 degrees; corresponding the south azimuth equal to 225 degrees and 135 degrees. The reason to choose the four angles is that each angle is the central angle of quadrant which can cover a circle perfectly. Based on the DEM, SRMs can be generated with different illumination azimuth angles. Figure 3.13 shows the SRMs of crater 1, Figures 3.13 (a) and (b) show the SRMs with an illumination azimuth angle of 315 ° and 45 °, respectively, and Figures 3.13 (c) and (d) show the SRMs with an illumination azimuth angle of 225 ° and 135 ° respectively. The sun elevation angles used for all these SRMs are 35 °. From Figure 3.13, it can be seen that the upper two SRMs have illumination directions from above which agrees with the light-from-above prior assumption and makes them look like craters, while the lower two have illumination directions from below which violates the light-from-above assumption and makes craters look like hillocks.

To get the most appropriate SRM for fusion, a more precise azimuth angle should be determined. As the northeast direction is easiest one for right judgment, 0 to 90 degrees range is supposed to be better. SRMs' azimuth angle (θ_1) could be varying due to the specific azimuth angle of satellite image (θ_0). Selection principle aims to

ensure that the illumination direction in both fused image will maintain an intersection angle of 45° so that they will not be offset by each other.

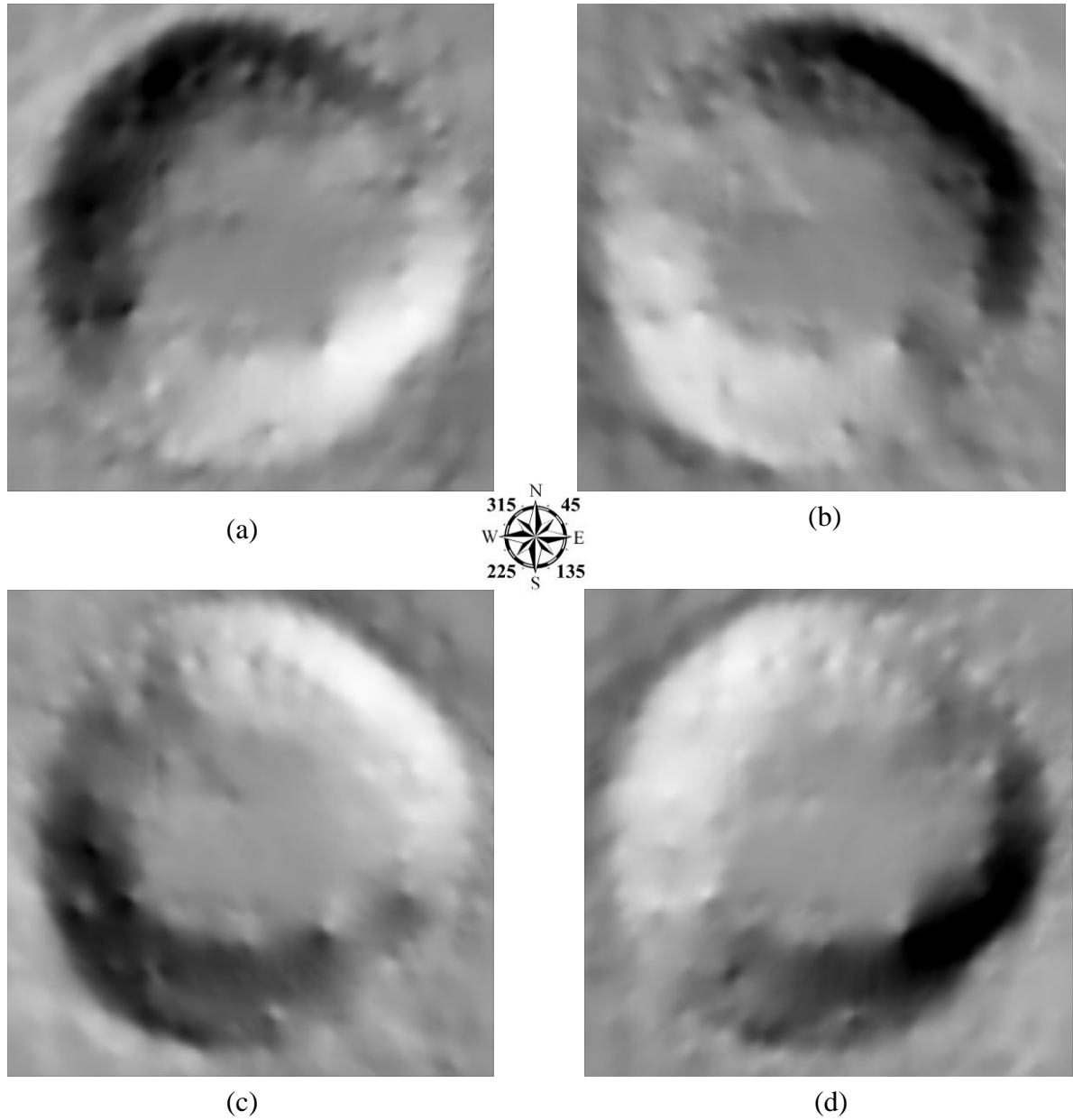


Figure 3.13 SRMs of Crater 1 generated based on the DEM with illumination azimuth angle of: (a) 315° , (b) 45° , (c) 225° , and (d) 135° .

The formula is:

$$|\theta_1 - \theta_0| = 225^\circ$$

Thus $\theta_1 = \theta_0 \pm 225^\circ$ ($0^\circ \leq \theta_1 < 90^\circ$)

As seen from Figure 3.14 (a), the light comes from either above or below. Considering the crater has the latitude of 55.33°N , the sunlight could only come from below, so that the original azimuth angle θ_0 is about 225° . According to the formula, the azimuth of SRM θ_1 should be: $225^\circ \pm 225^\circ = 0^\circ$ or 450° , where 450° equals to 90° ($450^\circ - 360^\circ = 90^\circ$). Considering the range of θ_1 , 0° is the suitable value.

The optimal sun elevation angle in generating these SRMs should be the same with that of the crater in the original image. The sun elevation angles for each row in the Chang'E-1 image are recorded in the meta data of the image, from which the sun elevation angles for specific craters can be derived

3.2.2 Image Fusion Based on the Shift Invariance Discrete Wavelet Transform (SIDWT)

Once the reference SRM images whose light comes from north are fixed, the next step is to fuse SRM with the original image.

The discrete wavelet transform (DWT) technology has been widely used in image fusion (Mallat, 1989; Rockinger, 1997).

From the visual system's point of view, human visual system is primarily sensitive to local contrast changes, whose contrast between features is corresponding to the image detail (Graps, 1995). The discrete wavelet transform (DWT) (Mallat, 1989) can decompose an image into its multi-scale representation in 2 dimensions. It is well known that, in general, wavelet-based technology perform better than standard methods such as intensity-hue-saturation (HIS) and principal component analysis (PCA), particularly in terms of minimizing colour distortion (Amolins et al., 2007). The main wavelet-based image fusion include the following three steps (Rockinger, 1997):

(1) The input images are decomposed by DWT to a multi-scale edge representation.

(2) A composite multi-scale representation is then built by selecting the most prominent wavelet coefficients in the input imagery. The selection is based on a simple maximization of the coefficients or a sophisticated area-based energy computation.

(3) Finally, the fused image computed by an inversed DWT to combine the wavelet representation to yield fusion images.

To generate stable and consistent fusion results, this study employed a shift invariant discrete wavelet transform (SIDWT) method (Rockinger, 1997; Sari-Sarraf and Brzakovic, 1997) for image fusion. The overall flowchart of the SIDWT method is illustrated in Figure 3.13. The SIDWT method was implemented in this study using Matlab, and the core source code can be found in the Appendix I.

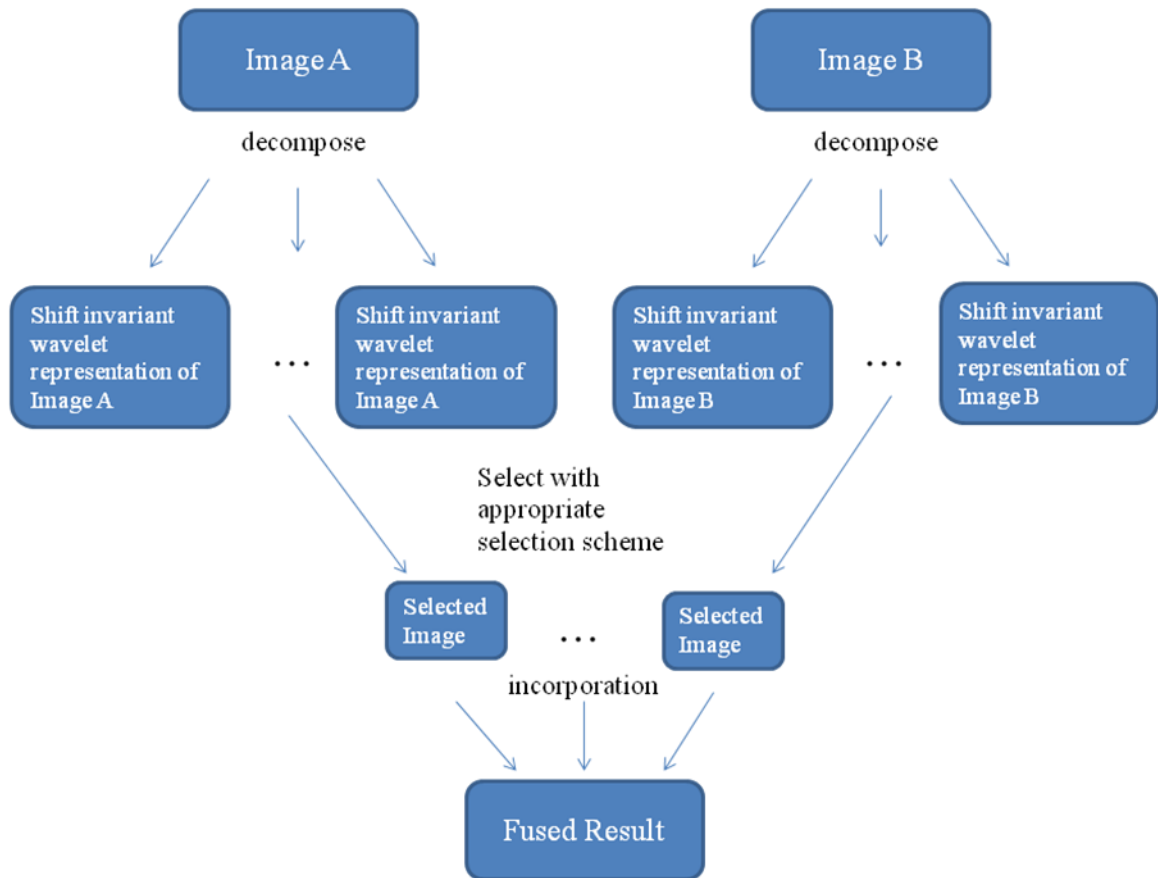


Figure 3.14 Flowchart of SIDWT

The wavelet-transform based approach was tested in this study. The fusion result of crater 1 is shown in Figure 3.15. The original image is fused with the SRM with an illumination azimuth angle of 0° (Figure 3.15(b)), and the results are shown in Figure 3.15(c). From the results, it is clear that the FTTP problem has been effectively alleviated as the objects shown as crater in the Figure 3.15 (c). However, if the corrected image is rotated by 180° , the FTTP problem will appear again, as shown in Figure 3.15(d). This wavelet-transform based approach is therefore only recommended for circumstances with no image rotation.

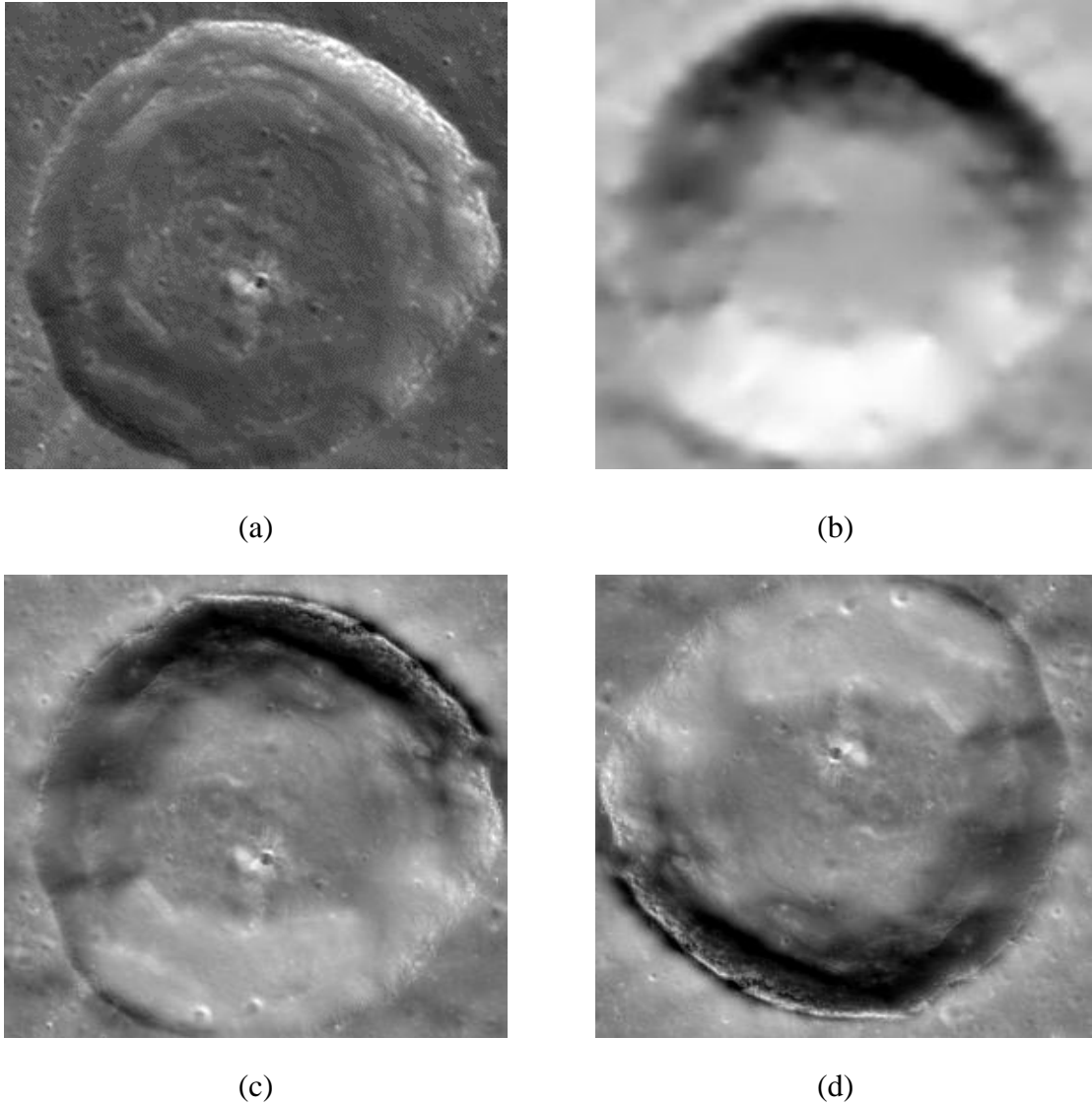


Figure 3.15 Fusion results images of Crater 1 using the wavelet-transform based approach: (a) the original image with FTTP, (b) SRM with azimuth angle of 0° , (c) the fused image free of FTTP, (d) the fused image rotated 180° with FTTP again

3.3 A Rotation Invariant Approach for Alleviation of FTTP Problems on Lunar Imagery

As mentioned in the former section, the wavelet-transform based approach is able to correct FTTP problems in lunar imagery effectively. However, the corrected images will suffer from FTTP again after rotating them upside down. This study developed the second approach for FTTP remediation on Chang'E-1 imagery, which is rotation invariant.

3.3.1 Motivation and Overview of the Approach

FTTP correction methods with rotation invariant were seldom discussed in the past, but rotation invariant is very important for FTTP correction since it helps to solve the false perception problem thoroughly in all circumstances. As reported in the literature review section, the FTTP is affected by the prior assumption of light-from-above (Ramachandran, 1988a; Toutin, 1998). However, this is not the only factor to perceive crater depth. Specular highlights and shadows are also suggested as strong visual cues to perceive depth (Mayhew and Longuet-Higgins, 1982; Todd and Norman, 2003; Todd, 2004). It was found that the darker area in the crater has greater depth than that in the bright area. Depth perception of human is a psychology process according to features of objects and the prior knowledge. The size, shadow and brightness are the features of objects in lunar satellite images, and shadow has

an important role to perceive depth. In Figure 3.16 (a), the center area rounded up by the inner small white circle is regarded as a concave area, for the human always has prior knowledge like that concave area is dark. Similar to Figure 3.16 (b), the Lambert crater is covered by a big dark shadow, which gives us a strong cue that light is illusion from right, and the central region is a crater. Figure 3.17 (a) shows another good example of a crater in a lunar image. A large dark shadow area is seen in the area, which indicates us that light is from the right and that the object is a crater. The image was rotated 90° for three times, and produced the images shown in Figure 3.17 (b), (c), and (d). It is observed from all these images that there is no FTTP problem and the object is still a crater regardless of the rotation angle. The light-from-above prior assumption is weak in this situation. The main reason here is that the shadow is the overwhelming cues to perceive the crater depth correctly. Based on theory of depth perception and observations, this study has developed a rotation invariant approach for FTTP remediation by incorporating the bright-darker gradient as a visual cue.

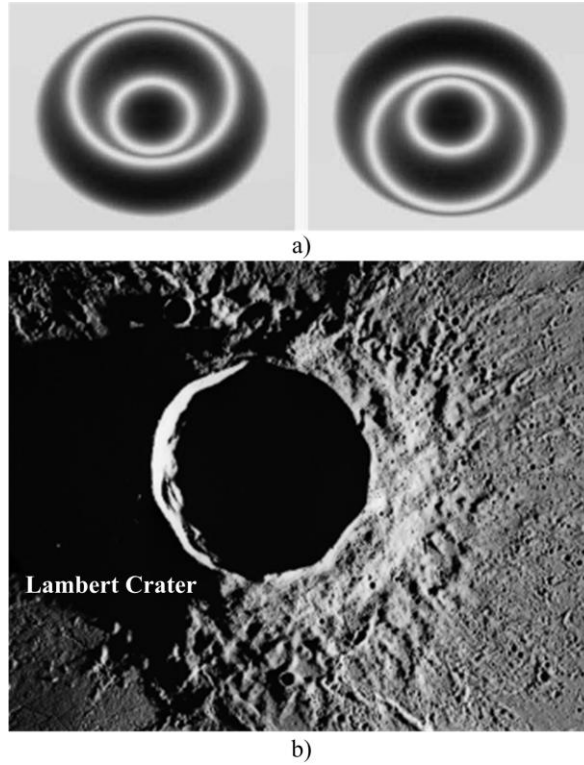


Figure 3.16 (a) Depth perception according to shade (Liu and Todd 2004), (b) Lambert crater remote sensing image from NASA covered by shadow

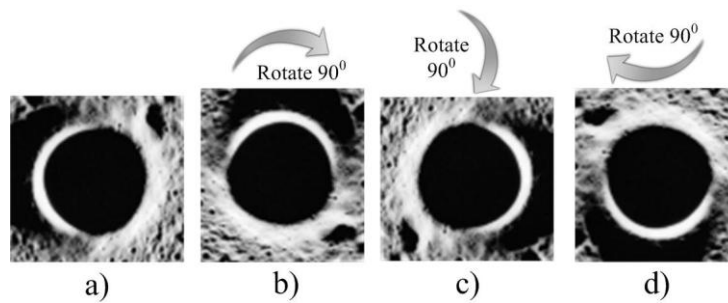


Figure 3.17 Symmetry structure with rotation invariant: (a) the original image, (b) image rotated 90° , (c) image rotated 90° again, and (d) image rotated 90° third time.

Similar to the wavelet-transform approach, crater DEMs generated from the integration of Chang'E-1 stereo imagery and the laser altimeter were employed for FTTP remediation in this approach. From the original crater image suffering from FTTP, the illumination direction can be determined. A SRM with an illumination direction opposite to the illumination direction of the original image can then be generated by using the crater DEM. An image fusion process was performed between the original image and the SRM using a SIDWT method, and an illumination balanced image was then derived. In the illumination balanced image, the brightness is homogenous and the FTTP problem on the balanced image is alleviated. A bright-darker gradient map was generated from the crater DEM, in which the bright to dark gradients represented places from high (crater rim) to low (crater bottom). The map was then fused with the illumination balanced image again using the SIDWT method, and the final crater image free of FTTP was generated which is rotation invariant. The overview of the approach is shown in Figure 3.18.

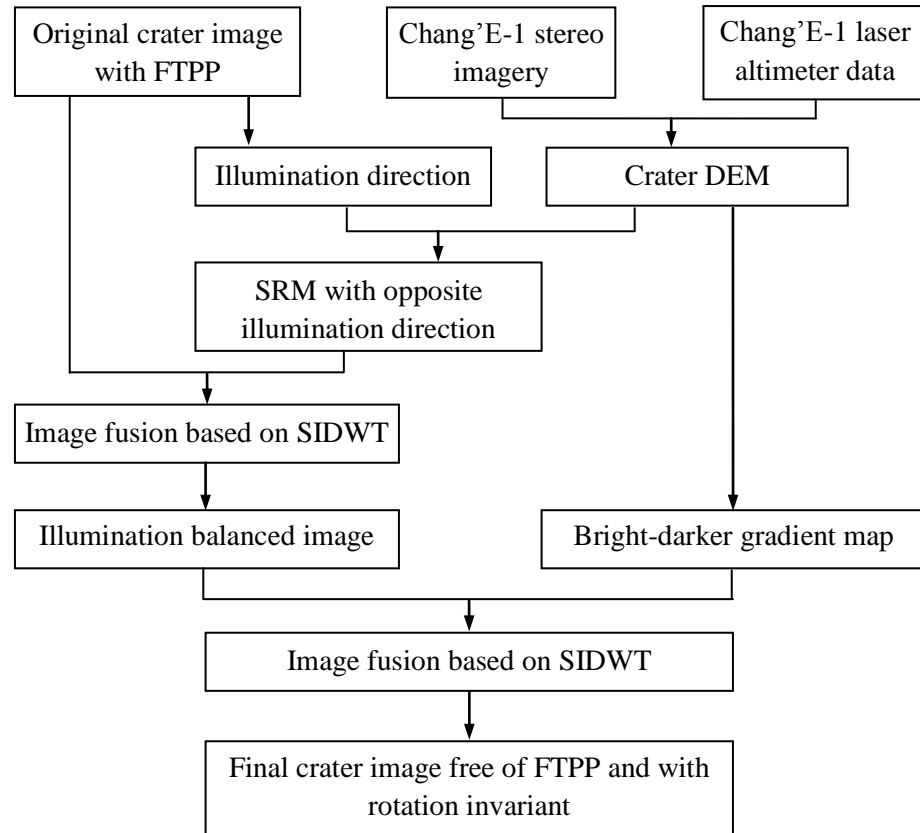


Figure 3.18 Overview of the rotation invariant approach

3.3.2 Illumination Balance

To achieve the veracity of the rotation invariant, the first step is to ensure that the illumination of crater image is balanced. This method aimed to use a SRM with the opposite illumination direction from the original image to fuse together. By doing this, the over-bright parts in the image could be covered by shadows and the shadows parts could also be balanced with illumination reflections.

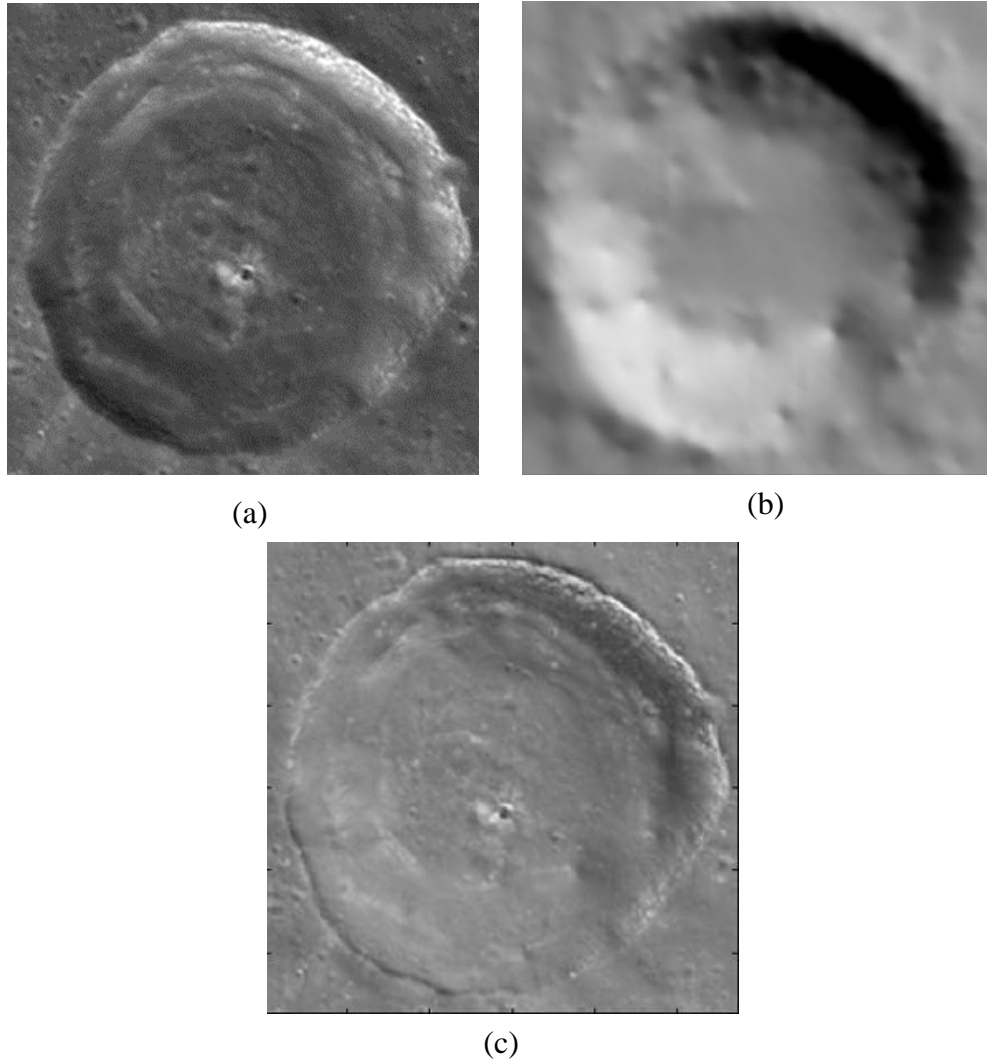


Figure 3.19 Crater 1 (a) original image, (b) SRM with azimuth angle of 45 °, (c) illumination balanced image

Figure 3.19 shows an illumination-balanced experiment for crater 1. As reported in the section of wavelet-transform approach, θ_0 of crater 1 is 225 °.

$$|\theta_2 - \theta_0| = 180^\circ \quad (0^\circ \leq \theta_2 \leq 90^\circ) \text{ or } (270^\circ \leq \theta_2 < 360^\circ)$$

According to above formula, azimuth angle of fused SRM θ_2 should be 45 ° (Figure

3.19 (b)) Figure 3.19 (c) shows the illumination balanced result of Crater 1. From the figure, it can be seen that the crater does not appear as a hillock compared to the original image in Figure 3.19 (a).

3.3.3 FTTP Remediation Invariant to Image Rotation

With the illumination balanced image, a bright-darker gradient map based on the crater DEM also needs to be generated for further processing. To achieve the best performance for image fusion, the grey scale of the bright-darker gradient map was designed to make sure that the inner area of the crater is darker and the area around the crater rim is brighter based on the crater depth information. Figure 3.20 (a) shows the bright-darker gradient map of crater 1. The map is then fused with the illumination balanced image using the SIDWT method. The result is the final crater image free of FTTP. Figure 3.20 (b) (c) (d) and (e) show the final results for crater 1.

Figure 3.20 (b) gives the result image. It can be seen that the bright-darker information is helpful in the perception of the crater depth, and the FTTP problem is alleviated compared with the original image illustrated in Figure 3.19 (a). The image textures remain after the fusion process. Figures 3.20 (c), (d), and (e) show the images after rotating the result image by 90° , 180° , and 270° respectively. In these images, the crater still looks like a crater.

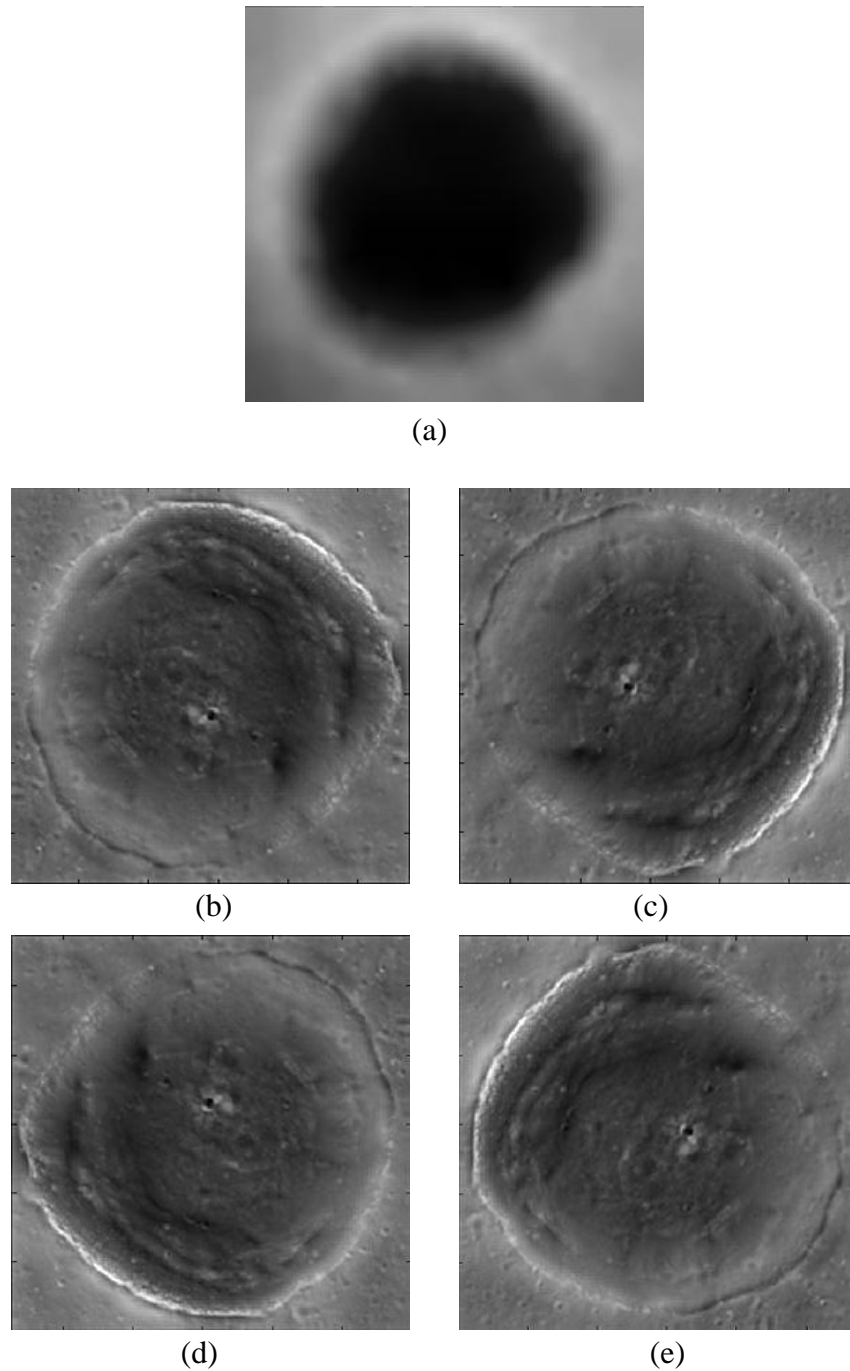


Figure 3.20 FTPP remediation for crater 1 using the rotation invariant approach: (a) the bright-darker gradient map, (b) the result image, (c) the result image rotated 90° , (d) rotated 180° , and (e) rotated 270° .

Chapter 4 Further Experiments and Evaluation

4.1 Further Experiments

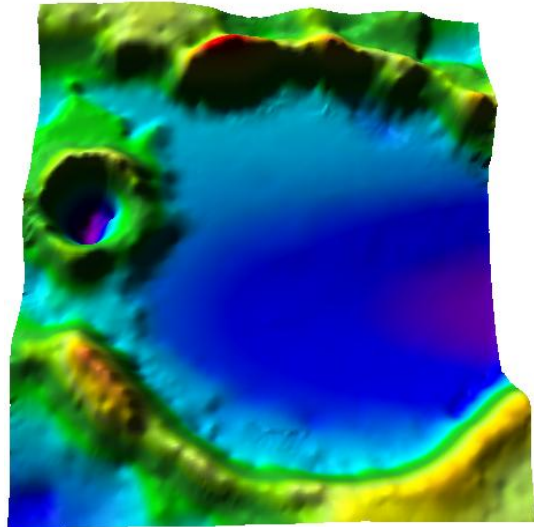
Two additional craters (craters 2 and 3) with different characteristics from crater 1 were tested using the two developed methods, which are the wavelet-transform based approach and the rotation invariant approach, to eliminate the FTPP problem.

4.1.1 Crater 2

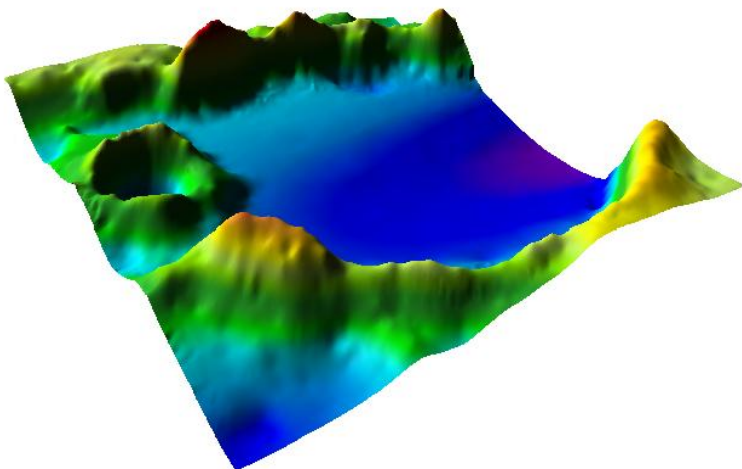
Crater 2 is located in 58.56 N, 86.96 E with a diameter of 52 km and depth of 0.8 km. Crater 2 is much flatter than crater 1. Figure 4.1 shows the original image of crater 2 and its DEMs from various views.



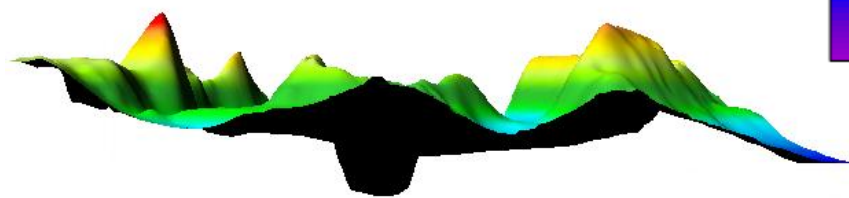
(a)



(b)



(c)



(d)

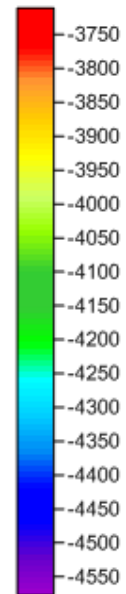


Figure 4.1 Crater 2 (a) the original image of crater 2, (b) overhead view of the DEM, (c) side view, (d) horizontal view

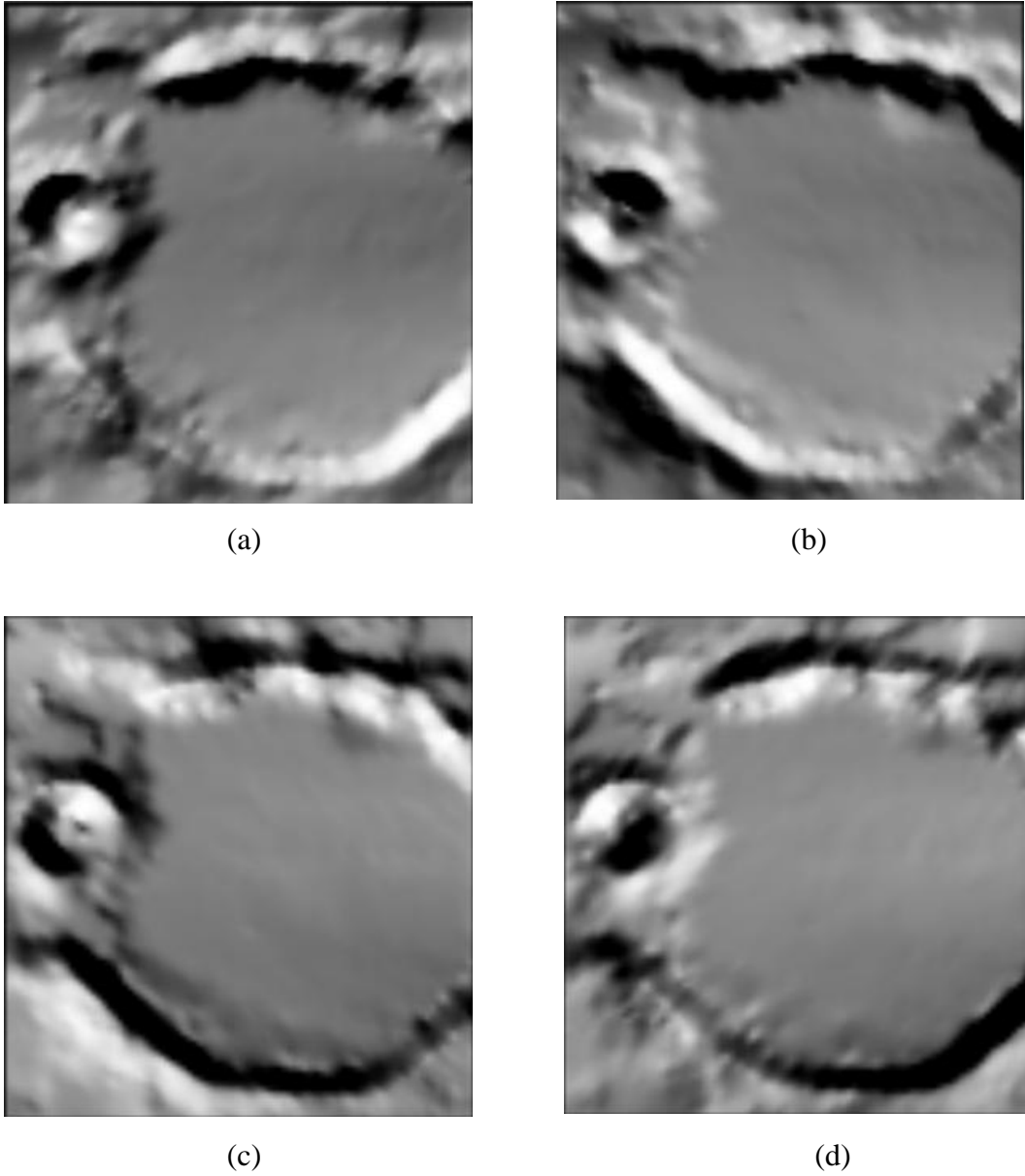


Figure 4.2 SRMs of Crater 2 generated based on the DEM with illumination azimuth angle of: (a) 315 °, (b) 45 °, (c) 225 °, and (d) 135 °.

Figure 4.2 is the SRMs of crater 2 with illumination azimuth angles of 45° , 135° , 225° and 315° respectively. As showed in Figure 4.1 (a), the light could come from either above or below (0° or 180°). Considering the crater is located in latitude of 58.56°N , the sunlight should only come from the south (below), so that the original azimuth angle θ_0 is about 180° . According to the formula from chapter 3, which is $\theta_1 = \theta_0 \pm 225^\circ$ ($0^\circ \leq \theta_1 < 90^\circ$), the azimuth of SRM θ_1 should be: $180^\circ \pm 225^\circ = -45^\circ$ or 405° , where 405° equals to 45° ($405^\circ - 360^\circ = 45^\circ$). Considering the range of θ_1 , 45° is the suitable value. By using the wavelet-transform based approach with the image showed in Figure 4.2 (b), an FTTP-free image for crater 2 was generated shown in Figure 4.3 (a). Figure 4.3 (b) is the image developed by rotating the image in Figure 4.3 (a) by 180° . It is seen that the FTTP problem appeared again after image rotation.

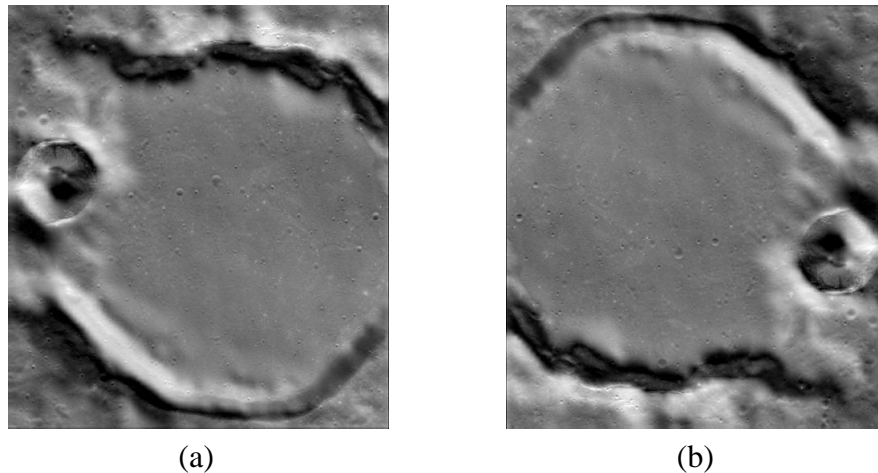


Figure 4.3 Fusion results of Crater 2 using the wavelet-transform based approach:

(a) the fused image free of FTTP, (b) the image rotated 180° with FTTP again

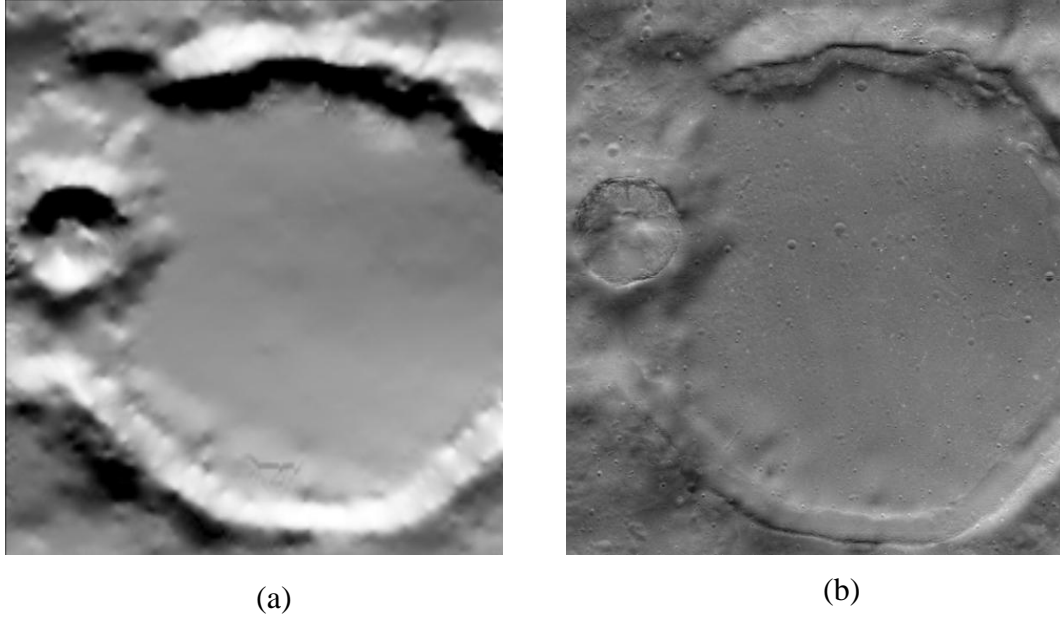


Figure 4.4 Crater 2 (a) SRM with azimuth angle of 0° , (b) Illumination balanced image

Another experiment for crater 2 was conducted by using the rotation invariant approach. In the first step, an illumination balanced image was generated by fusing with an opposite illumination SRM. As the original azimuth angle θ_0 is about 180° , the azimuth angle of SRM should be 0° ($|\theta_2 - \theta_0| = 180^\circ$ ($0^\circ \leq \theta_2 \leq 90^\circ$) \cup ($270^\circ \leq \theta_2 < 360^\circ$)). Figure 4.4 (a) shows the SRM with azimuth angle of 0° , and Figure 4.4(b) gives the result of illumination balanced image. Figure 4.5 shows the bright-darker gradient map of crater 2 and the image results using the rotation invariant approach. Figure 4.5 (b) is the direct result image. Figure 4.5 (c), (d), and (e) are the images after rotating the result image by 90° , 180° , and 270° respectively. The FTTP problems in these images are alleviated compared with those shown in the original image as shown in Figure 4.1 (a).

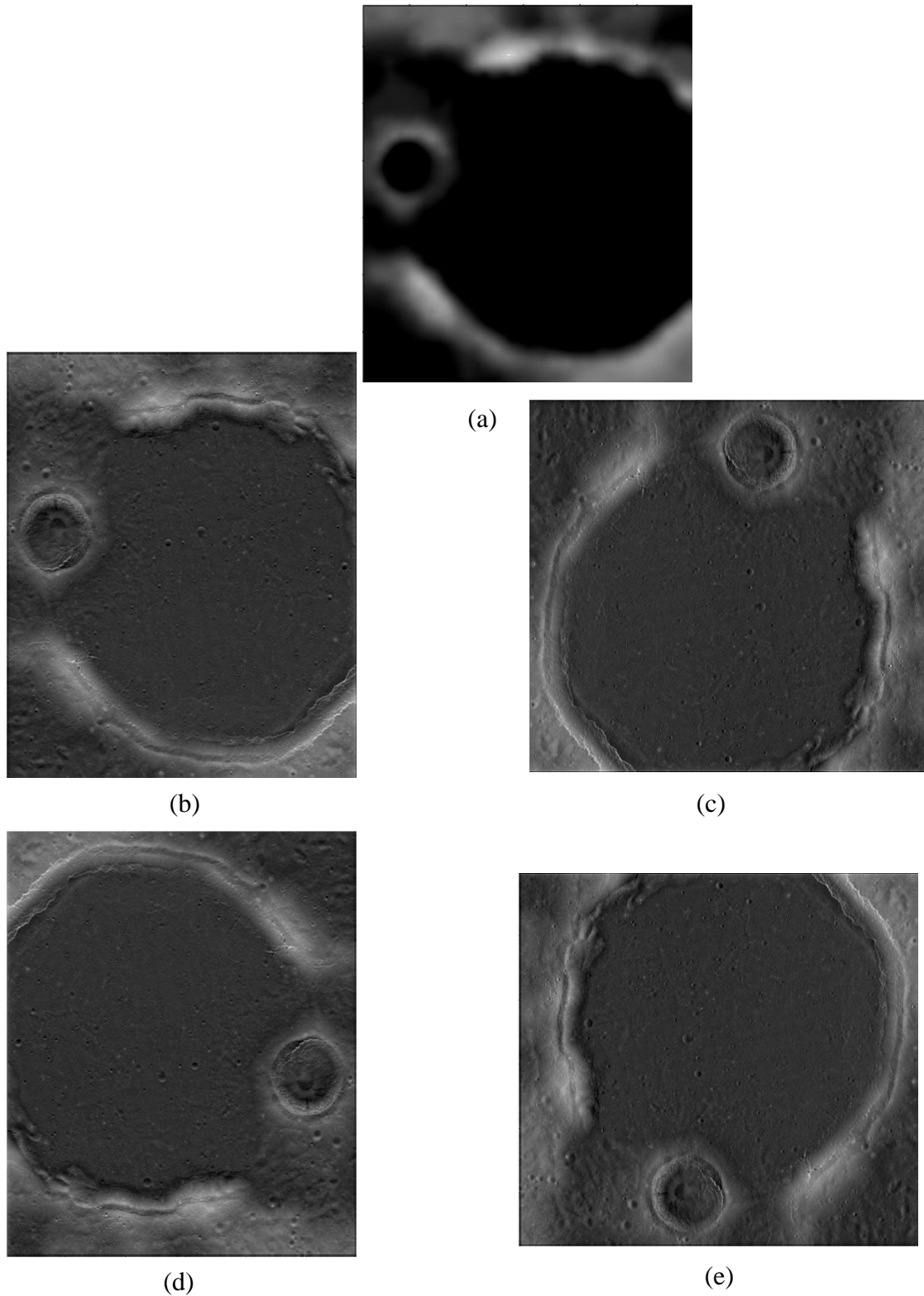


Figure 4.5 FTTP remediation for Crater 2 using the rotation invariant approach:

(a) the bright-darker gradient map, (b) the result image, (c) the result image rotated 90 °, (d) rotated 180 ° and (e) rotated 270 °

4.1.2 Crater 3

Crater 3 is located in 55.33 °N, 118.33 °W with a diameter of 32 km and depth of 3.5 km. This crater has a similar size and shape compared to crater 1, but gets more illumination exposure than crater 1. Figure 4.6 shows the original image of crater 3 and its DEMs. Figure 4.7 is the SRMs of crater 3 with the illumination azimuth angle of 45 °, 135 °, 225 ° and 315 ° respectively.

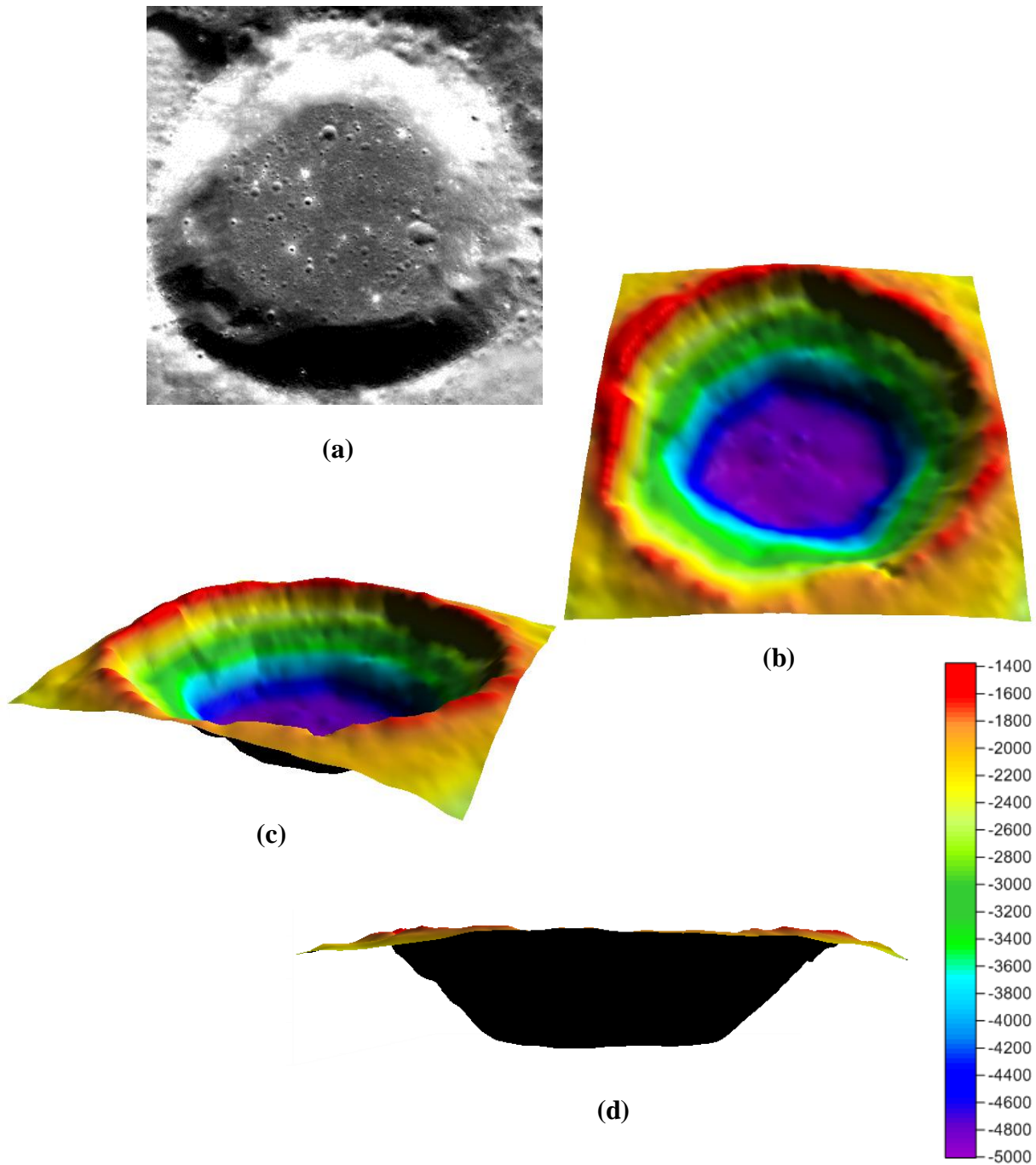


Figure 4.5 Crater 3 (a) the original image of Crater 3, (b) overhead view of the DEM, (c) side view, (d) horizontal view

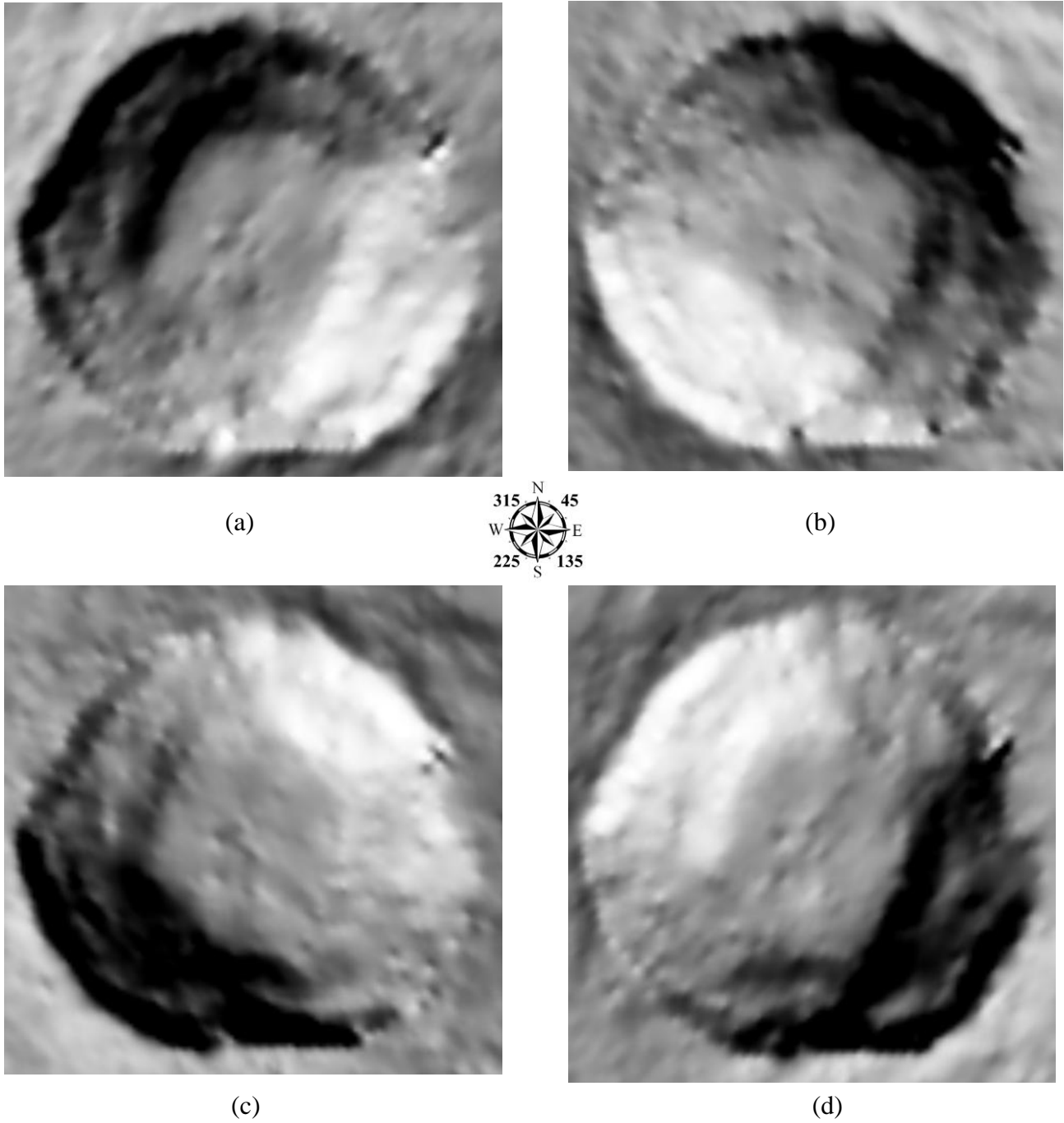


Figure 4.7 SRMs of Crater 3 generated based on the DEM with illumination azimuth angle of: (a) 315 °, (b) 45 °, (c) 225 °, and (d) 135 °

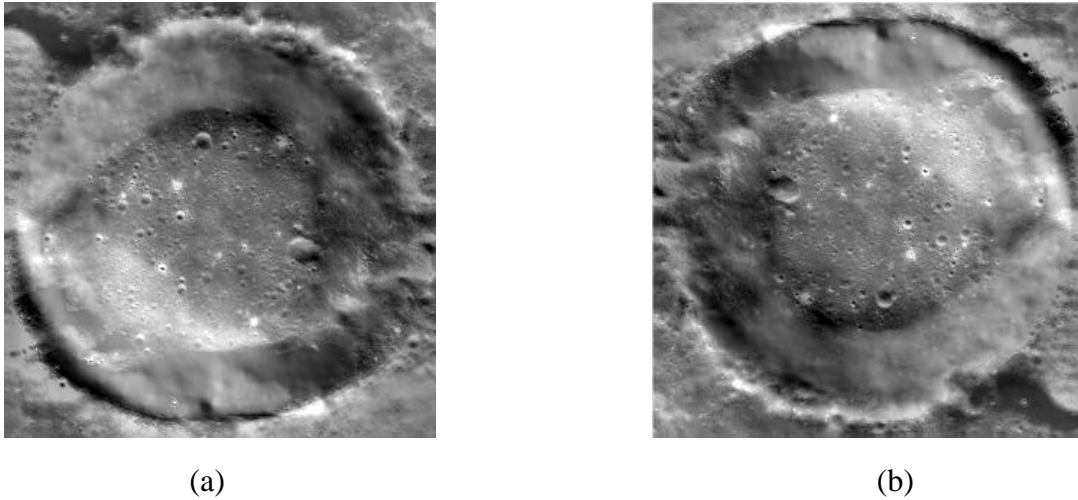
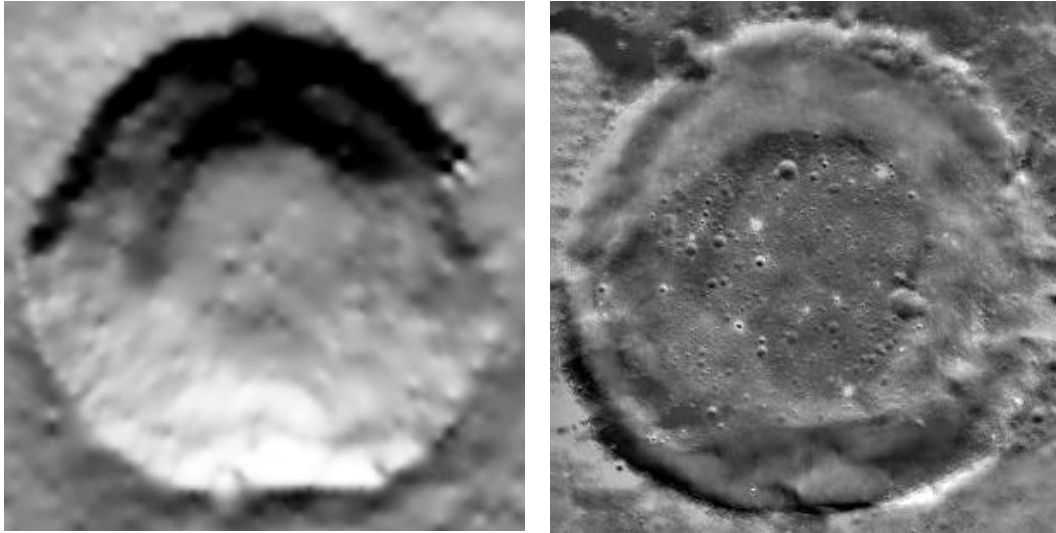


Figure 4.8 Fusion results for crater 3 using the wavelet-transform based approach: (a) the fused image free of FTPP, (b) the fused image rotated 180° with FTPP again.

As shown in Figure 4.6 (a), the incident light direction had two possibilities which were the north and the south. Considering the crater has the latitude of 55.33°N , the sunlight could only come from below (the south direction). So that the original azimuth angle θ_0 is about 180° . According to the formula $\theta_1 = \theta_0 \pm 225^\circ$ ($0^\circ \leq \theta_1 < 90^\circ$), the azimuth of SRM θ_1 should be: $180^\circ \pm 225^\circ = -45^\circ$ or 405° , where 405° equals to 45° ($405^\circ - 360^\circ = 45^\circ$). Considering the range of θ_1 , 45° is the suitable value. Figure 4.7 (b) shows the SRM with the azimuth angle of 45° . By using the wavelet-transform based approach, an FTPP-free image for crater 3 is generated as shown in Figure 4.8 (a). Figure 4.8 (b) presents the resulting image by rotating the image in Figure 4.8 (a) by 180° , indicating that the FTPP problem appears.



(a)

(b)

Figure 4.9 Crater 3 (a) SRM with azimuth angle of 0° , (b) illumination balanced image

To obtain the illumination balanced image, another image fusion process is needed. As the original azimuth angle θ_0 is about 180° , an opposite illumination SRM should be generated with azimuth angle of 0° ($|\theta_2 - \theta_0| = 180^\circ$ ($0^\circ \leq \theta_2 \leq 90^\circ$) \cup ($270^\circ \leq \theta_2 < 360^\circ$)). Figure 4.9 (a) shows this SRM with azimuth angle of 0° , and Figure 4.9 (b) gives the result of illumination balanced image. The image in Figure 4.10 (a) is the bright-darker gradient map of crater 3, and Figure 4.10 (b) shows the direct results using the rotation invariant approach. Figures 4.10 (c), (d) and (e) present the images after rotating the result image by 90° , 180° , and 270° respectively. The FTPP problems in these images are alleviated compared with the original image as shown in Figure 4.6 (a).

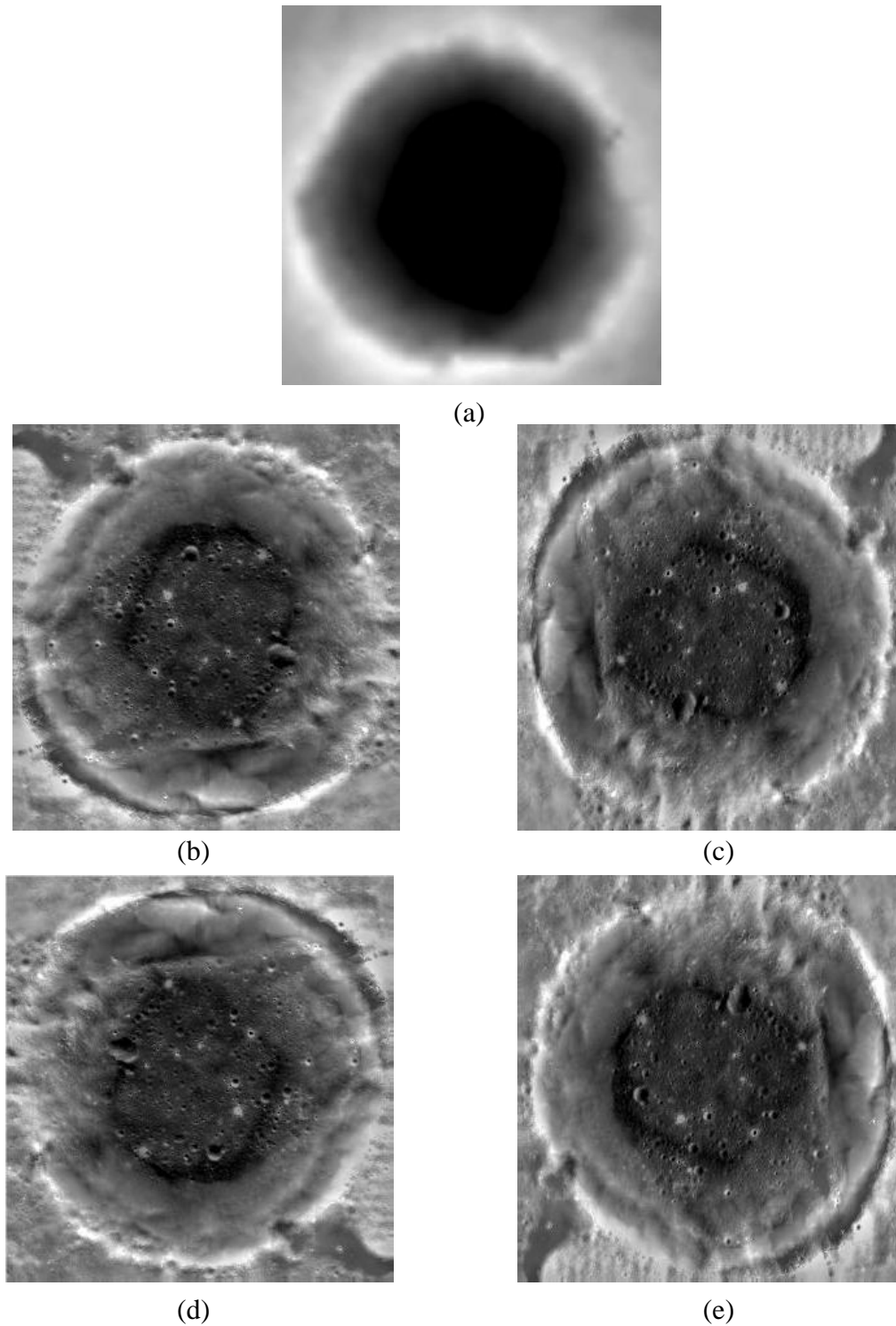


Figure 4.10 FTPP remediation for Crater 3 using the rotation invariant approach: (a) the bright-darker gradient map; (b) the result image; (c) the result image rotated 90° ; (d) rotated 180° and (e) rotated 270°

4.2 Evaluation

To evaluate the performances of the two methods presented in this paper, a questionnaire survey was carried out with 31 people who have various remote sensing backgrounds and no previous knowledge of FTPP. The questionnaire contained 15 questions. Subjects had to identify the FTPP levels of each of the three craters tested in this study under five different conditions. They were image 1 (the original image), image 2 (the image after FTPP correction using the wavelet-transform approach), image 3 (rotating the image 2 by 180°), image 4 (the image after FTPP remediation using the rotation invariant approach), and image 5 (rotating the image 4 by 180°). The FTPP levels were classified following the scheme given above: levels 5, 6, 7, 8, and 9 with 5 representing light FTPP and 9 representing heavy FTPP), while the other four levels were added to evaluate the depth perception strength (levels 1, 2, 3, and 4 with 1 representing strong depth perception and 4 representing relatively weak depth perception). The example of the questionnaire is shown represented in Appendix II. The findings of the survey are summarized in Table 4.

Table 4 Summary of the survey findings

		Image 1 (original image)	Image 2 (wavelet- transform approach)	Image 3 (rotating image 2 by 180 °)	Image 4 (rotation invariant approach)	Image 5 (rotating image 4 by 180 °)
Crater 1	Average	6.18	3.34	6.00	3.50	4.18
	Stdev	1.42	1.72	1.52	1.31	1.62
Crater 2	Average	5.96	3.82	5.62	3.86	4.52
	Stdev	0.56	0.89	0.63	0.70	0.99
Crater 3	Average	7.34	2.8	6.16	3.52	4.20
	Stdev	2.01	1.73	1.74	1.19	1.42

From Table 4, it is clearly seen that the three experimental craters all contain FTPP problems, with the average FTPP levels, as judged by the 31 interviewees, to be all larger than 5. After remediation using the wavelet-transform approach, the FTPP levels dropped to 3.34, 3.82 and 2.8. This indicates that the wavelet-transform approach works effectively. After image rotation of 180 °, however, the FTPP levels increased to 6, 5.62, and 6.16, which agrees with the statement referred in the section 3.2.2 that image rotation would reverse the remediation result of the wavelet-transform approach. In the image 4 column, the rotation invariant approach took the FTPP levels to 3.5, 3.86, and 3.52. After rotation of 180 °, these values changed to 4.18, 4.52, and 4.2. A comparison of these two sets of values reveals that they are slightly increased with the rotation of 180 ° but still kept below 5. Table 4 also lists

the standard deviations for each case. Here it can be seen that the responses from the interviewees are quite consistent for crater 2 and relatively dispersed for craters 1 and 3. A comparison of the results using the wavelet-transform based approach with that of the rotation invariant approach reveals that the remediation effects are similar with the former being slightly better. However, after image rotation, the rotation invariant approach still worked while the wavelet-transform based approach did not.

Chapter 5 Conclusions and Discussion

This research aimed to investigate the False Topographic Perception Phenomena (FTPP) observed on the imagery of the Moon's surface acquired by the lunar orbiting satellites (Chang'E-1). It has systematically investigated the FTTP problem observed on the Chang'E-1 imagery. The factors related to the FTTP problem have been analyzed. It was found that the FTTP problem was positively correlated to the latitude of the terrain features, and majority of the objects suffering with the FTTP problem on the Chang'E-1 imagery are in the north hemisphere.

To alleviate the FTTP on the lunar orbiter imagery, several traditional methods were investigated, which included the image rotation method, Digital Number (DN) invert method and the Shaded Relief Model (SRM) method. The image rotation method and Digital Number (DN) invert method applied in this study are similar with the previous ways to treat with the Earth imagery. For the wavelet-transform method, this study uses a new Shift Invariance Discrete Wavelet Transform (SIDWT) fusion way to deal with the one band lunar orbiter imagery. Experimental results showed advantages and disadvantages of using these three methods.

An illumination elimination method using the wavelet-transform approach is

developed to better alleviate the FTTP problem. All the existing FTTP correction methods are focused on changing the illumination direction to upper according to “light-from-above” nature. In that case, the observation direction could not be changed after the correction. FTTP could appear again by either image rotation or movement of the map viewer. The only way to remediate FTTP completely is to remove the shadow information caused by the incident light. Digital terrain models were generated using Chang’E-1 imagery, and SRMs with the illumination direction opposite to the original incident sunlight were derived. Image fusion was then performed using the Shift Invariance Discrete Wavelet Transform (SIDWT) technology between the original orbiter image and the SRMs. After these procedures, images free of FTTP can be obtained.

Depth maps were fused with the FTTP free images to improve the performance of the rotation invariant treatment for FTTP. Although the FTTP has been alleviated by illumination elimination, the concave and convex are not so obviously by lack of shadows. Reconstruction of depth information needs to be carried according to the “darker-represent-lower” nature. A depth map could generate by DEM using various DN values. Second time fusion between depth map and previous illumination eliminate result was performed. By doing these, enhanced final result of rotation invariant image could be got which shows the effective performance of the proposed method.

Research analytical analysis was carried out with three sets of craters. Each set of data contained three images in the order of original image, FTTP eliminated image with the wavelet-transform based approach, and the FTTP eliminated one with rotation invariant approach. After individual analysis, these data were represented to 31 interviewees with various remote sensing backgrounds to get objective feedbacks. The statistic result supports the analytical outcomes, which are the remediation effects of the wavelet-transform based approach and the rotation invariant approach are similar with the former being slightly better. However, after image rotation, the rotation invariant approach still worked while the wavelet-transform based approach did not.

5.1 Conclusions

This study presents a systematic investigation of the FTTP problem observed in the Chang'E-1 lunar imagery and also presents effective methods for FTTP remediation.

The analysis and experimental results lead to the following conclusions:

- (1). The FTTP problem associated with craters revealed by lunar imagery is positively correlated with the latitudes of craters in the northern hemisphere of the Moon, and for craters within similar latitude ranges. the FTTP level is positively correlated with the depth-diameter ratio of the crater;

- (2). The wavelet-transform based approach is able to correct FFTP problems effectively, but is only recommended for circumstances with no image rotation;
- (3). The rotation-invariant approach is also capable of correcting the FFTP problem, which is not subject to image rotation. It is suitable for applications such as using the lunar surface images for navigation or exploration of the lunar surface using software systems such as Google Moon.

5.2 Discussion and Future Work

The experiment data used in this research are mainly based on Chang'E-1 satellite imagery, as the lunar orbiter imagery data could not be accessed easily. The research will be more complete and comprehensive if it covers more FFTP alleviation experiments by using more other lunar satellites data such as SELENE and Chandrayaan-1.

Comparing the FTPP remediated images by the wavelet-transform based approach and the rotation invariant approach with the original images for craters 1, 2, and 3, it can be noticed that the remediation process may cause slight deviations from the exact perception of the crater morphology. However, the described remediation method is still valuable since it corrects FTPP problems to avoid obvious wrong perceptions.

The wavelet-transform based approach requires DEMs with good resolutions. The resolution of DEM generated from the Chang'E-1 imagery is surely lower than that of the original images. To improve the performance of the developed method in this aspect will be our future efforts. Our future work will use DEMs from other high resolution data sources such as the Chang'E-2 and LRO imagery.

The remediation effects of the rotation invariant approach are not as effective as that of the wavelet-transform based one. To eliminate the influence of illumination, it was balanced in the first step of this approach. After this processing, the image looked much flatter than before without the shadows. By using with the bright-darker gradient map, perception of depth is recurrent but weaker than before. Thus the direct FTPP alleviated results may be not as obvious as those of the wavelet-transform based method. But the overall performance of the rotation invariant approach is promising since it is rotation invariant. Our future efforts will be put to improve the depth perception of rotation invariant approach.

It should be noted that, this investigation is based on the selected study areas covering the latitudes from -70° to 70° of the lunar surface. The extreme cases in the North Pole region are not included in this investigation. A systematic investigation about the FTTP problems in the North Pole region and generation of crater DEMs with favorable resolution from other data source (e.g., the LRO NAC images or Laser Altimeter data) for FTTP remediation in the North Pole region will be our future efforts.

References

References

- Amolins, K., Y. Zhang, and P. Dare (2007), Wavelet based image fusion techniques - An introduction, review and comparison. *ISPRS Journal of Photogrammetry and Remote Sensing*, 62[4], 249-263.
- CAS (Chinese Academy of Sciences) (2008), Working References for the Lunar Explorer Project Scientific Application Users, Chinese Academy of Sciences, Lunar Exploration Project, General Design Section, 140 p.
- Colby, J. D. (1991), Topographic normalization in rugged terrain, *Photogrammetric Engineering and Remote Sensing*, 57[5], 531-537.
- Drury, S. A. (1987), *Image Interpretation in Geology*, Allen & Unwin: London.
- Graps, A. (1995), An introduction to wavelets, *IEEE Computational Science and Engineering*, 2[2], 50-61.
- Ivanov, B. A. (2001), Mars/Moon Cratering Rate Ratio Estimates, *Chronology and Evolution of Mars*, 96, 87-104.
- Kumar, A. S. K., and A. R. Chowdhury (2005), Terrain mapping camera for Chandrayaan-1, *Journal of Earth System Science*, 114 [6], 717-720.
- Lillesand, T. M. and Kiefer, R. W. (1979), *Remote Sensing and Image Interpretation*, John Wiley: New York.
- Liu, B., and J. T. Todd (2004), Perceptual biases in the interpretation of 3D shape from shading, *Visual Research*, 44[18], 2135-2145.

References

- Mallat, S. G. (1989), A theory for multiresolution signal decomposition: the wavelet representation, *IEEE Transactions on Pattern Analysis and Machine Intelligence*, 11[7], 674-693.
- Mayhew, J. E. W., and H. C. Longuet-Higgins (1982), A computational model of binocular depth perception, *Nature*, 297, 376-378.
- Morgenstern, Y., R. F. Murray, and L. R. Harris (2011), The human visual system's assumption that light comes from above is weak, *Proceedings of the National Academy of Sciences of the United States of America (PNAS)*, 108, 12551-12553.
- Moutsoulas, M., and P. Preka (1981), Morphological characteristics of lunar craters with moderate depth/diameter ratio, *Earth, Moon, and Planets*, 25[1], 51-66.
- Ouyang, Z. Y., C. Li, Y. Zou, H. Zhang, C. Lv, J. Liu, J. Liu, W. Zuo, Y. Su, and W. Wen (2010), Preliminary scientific results of Chang'E-1 lunar orbiter, *Science China*, 53[11], 1565–1581.
- Patterson, T., and N. V. Kelso (2004), Hal Shelton Revisted: Designing and Producing Natual-Color Maps with Satellite Land Cover Data, *Cartographic Perspectives*, 47, 28-55.
- Ramachandran, V. S. (1988a), Perception of shape from shading, *Nature*, 331[6152], 133-166.
- Ramachandran, V. S. (1988b), Perceiving shape from shading, *Scientific American*, 259[2], 76-83.
- Rieser, J. J., H. L. Pick, D. H. Ashmead, and A. E. Garing (1995), Calibration of human locomotion and models of perceptual motor organization, *Journal of*

References

- Experimental Psychology: Human Perception and Performance*, 21[3], 480-497.
- Robinson, M. S., S. M. Brylow, M. Tschimmel, D. Humm, S. J. Lawrence, P. C. Thomas, B. W. Denevi, E. Bowman-Cisneros, J. Zerr, M. A. Ravine, M.A. Caplinger, F.T. Ghaemi, J.A. Schaffner, M.C. Malin, P. Mahanti, A. Bartels, J. Anderson, T.N. Tran, E.M. Eliason, A.S. McEwen, E. Turtle, B.L. Jolliff, and H. Hiesinger (2010), Lunar Reconnaissance Orbiter Camera (LROC) Instrument Overview, *Space Science Reviews*, 150[1-4], 81-124.
- Rockinger, O. (1997), Image sequence fusion using a shift-invariant wavelet transform: Proceedings 1997 International Conference on Image Processing (ICIP '97), p. 288-291.
- Rudnicki, W. (2000), The new approach to the relief shading applied in the satellite image maps, Proceedings of the Second Symposium of the Commission on Mountain Cartography, p. 105-106.
- Saraf, A. K., J. Das, B. Agarwal, and R. M. Sundaram (1996), False topography perception phenomena and its correction, *International Journal of Remote Sensing*, 17[18], 3725-3733.
- Saraf, A. K., P. Ghosh, B. Sarma, and S. Choudhury (2005), Development of a new image correction technique to remove false topographic perception phenomena, *International Journal of Remote Sensing*, 26[8], 1523-1529.
- Saraf, A. K., S. T. Sinha, P. Ghosh, and S. Choudhury (2007), A new technique to remove false topographic perception phenomenon and its impacts in image interpretation, *International Journal of Remote Sensing*, 28[5], 811-821.

References

- Saraf, A. K., M. Zia, J. Das, K. Sharma, and V. Rawat (2011), False topographic perception phenomena observed with the satellite images of Moon's surface, *International Journal of Remote Sensing*, 32[24], 9869-9877.
- Sari-Sarraf, H., and D. Brzakovic (1997), A shift-invariant discrete wavelet transform, *IEEE Transactions on Signal Processing*, 45[10], 2621-2626.
- Sheffield, C (1986), *Earthwatch: A Survey of the World from Space*, Octopus Books: London.
- Stepinski, T. F. (2010), Geographical Distribution of Crater Depths on Mars, *Proceeding of the 41st Lunar and Planetary Science Conference*, The Woodlands, Texas, March 1-5, 2010.
- Todd, J. T. (2004), The visual perception of 3D shape, *Trends in Cognitive Sciences*, 8[3], 115-121.
- Todd, J. T., and J. F. Norman (2003), The visual perception of 3-D shape from multiple cues: are observers capable of perceiving metric structure? *Perception & Psychophysics*, 65[1], 31-47.
- Toutin, T. (1998), Depth perception with remote sensing data, In *Future Trends in Remote Sensing* (edited by P. Gudmandsen: A.A. Balkema), pp. 401-409.
- Wu, B., J. Guo, Y. Zhang, B. King, Z. Li, and Y. Chen (2011), Integration of Chang'E-1 Imagery and Laser Altimeter Data for Precision Lunar Topographic Modeling, *IEEE Transactions on Geoscience and Remote Sensing*, 49(12): 4889 - 4903.

Appendix I

Core source code for the Shift Invariance Discrete Wavelet Transform (SIDWT)

method

```
Function Y = fuse_sih(M1, M2, zt, ap, mp)
% Y = fuse_sih(M1, M2, zt, ap, mp) image fusion with SIDWT, Wavelet is Haar
%
% M1 - input image A
% M2 - input image B
% zt - maximum decomposition level
% ap - coefficient selection highpass (see selc.m)
% mp - coefficient selection base image (see selb.m)
%
% Y - fused image

% (This method developed by Oliver Rockinger 16.08.99)

% check inputs
[z1 s1] = size(M1);
```

Appendix I

```
[z2 s2] = size(M2);

if (z1 ~= z2) | (s1 ~= s2)

    error('Input images are not of same size');

end;

% cells for selected images

E = cell(3,zt);

% loop over decomposition depth -> analysis

for i1 = 1:zt

    % calculate and store actual image size

    [z s] = size(M1);

    zl(i1) = z; sl(i1) = s;

    % define actual filters (inserting zeros between coefficients)

    h1 = [zeros(1,floor(2^(i1-2))), 0.5, zeros(1,floor(2^(i1-1)-1)), 0.5,
zeros(1,max([floor(2^(i1-2)),1]))];

    g1 = [zeros(1,floor(2^(i1-2))), 0.5, zeros(1,floor(2^(i1-1)-1)), -0.5,
zeros(1,max([floor(2^(i1-2)),1]))];

    fh = floor(length(h1)/2);

    % image A

    Z1 = conv2(es(M1, fh, 1), g1, 'valid');

    A1 = conv2(es(Z1, fh, 2), g1, 'valid');
```

Appendix I

```
A2 = conv2(es(Z1, fh, 2), h1', 'valid');
Z1 = conv2(es(M1, fh, 1), h1, 'valid');
A3 = conv2(es(Z1, fh, 2), g1', 'valid');
A4 = conv2(es(Z1, fh, 2), h1', 'valid');
% image B
Z1 = conv2(es(M2, fh, 1), g1, 'valid');
B1 = conv2(es(Z1, fh, 2), g1', 'valid');
B2 = conv2(es(Z1, fh, 2), h1', 'valid');
Z1 = conv2(es(M2, fh, 1), h1, 'valid');
B3 = conv2(es(Z1, fh, 2), g1', 'valid');
B4 = conv2(es(Z1, fh, 2), h1', 'valid');

% select coefficients and store them
E(1,i1) = {selc(A1, B1, ap)};
    E(2,i1) = {selc(A2, B2, ap)};
    E(3,i1) = {selc(A3, B3, ap)};

    % copy input image for next decomposition stage
M1 = A4;
M2 = B4;
end;

% select base coefficients of last decomposition stage
```

Appendix I

```
A4 = selb(A4,B4,mp);
```

```
% loop over decomposition depth -> synthesis
```

```
for i1 = zt:-1:1
```

```
    % define actual filters (inserting zeros between coefficients)
```

```
    h2 = fliplr([zeros(1,floor(2^(i1-2))), 0.5, zeros(1,floor(2^(i1-1)-1)), 0.5,  
zeros(1,max([floor(2^(i1-2)),1]))]);
```

```
    g2 = fliplr([zeros(1,floor(2^(i1-2))), 0.5, zeros(1,floor(2^(i1-1)-1)), -0.5,  
zeros(1,max([floor(2^(i1-2)),1]))]);
```

```
    fh = floor(length(h2)/2);
```

```
    % filter (rows)
```

```
    A4 = conv2(es(A4, fh, 2), h2, 'valid');
```

```
    A3 = conv2(es(E{3,i1}, fh, 2), g2, 'valid');
```

```
    A2 = conv2(es(E{2,i1}, fh, 2), h2, 'valid');
```

```
    A1 = conv2(es(E{1,i1}, fh, 2), g2, 'valid');
```

```
    % filter (columns)
```

```
    A4 = conv2(es(A4+A3, fh, 1), h2, 'valid');
```

```
    A2 = conv2(es(A2+A1, fh, 1), g2, 'valid');
```

```
    % add images
```

```
    A4 = A4 + A2;
```

```
end;
```

Appendix I

% copy image

Y = A4;

Appendix II

Appendix II

Sample of the Questionnaire Survey

Here is a scanned copy for one of the questioners. (3pages)

Every page contains five images from the crater 1, crater 2 and crater3 respectively, and they are the original satellite image, wavelet-transform based approached one, 180 °rotated wavelet-transform based approached one, rotation invariant approached one and 180 °rotated rotation invariant approach one sequentially.

Appendix II

Crater 1

Questionnaire LS09

1. Does this object apex or concave? Please give your prefer number.

Extremely Concave Flat Extremely Apex
1 2 3 4 5 6 **7** 8 9

Questionnaire LS09

2. Does this object apex or concave? Please give your prefer number.

Extremely Concave Flat Extremely Apex
1 **2** 3 4 5 6 7 8 9

Questionnaire LS09

3. Does this object apex or concave? Please give your prefer number.

Extremely Concave Flat Extremely Apex
1 2 3 4 5 6 **7** 8 9

Questionnaire LS09

4. Does this object apex or concave? Please give your prefer number.

Extremely Concave Flat Extremely Apex
1 2 **3** 4 5 6 7 8 9

Questionnaire LS09

5. Does this object apex or concave? Please give your prefer number.

Extremely Concave Flat Extremely Apex
1 2 **3** 4 5 6 7 8 9

Appendix II


Crater 2

Questionnaire

6. Does this object apex or concave? Please give your prefer number.

Extremely Concave Flat Extremely Apex

1 2 3 4 5 6 7 8 9




Questionnaire

7. Does this object apex or concave? Please give your prefer number.

Extremely Concave Flat Extremely Apex

1 2 3 4 5 6 7 8 9




Questionnaire

8. Does this object apex or concave? Please give your prefer number.

Extremely Concave Flat Extremely Apex

1 2 3 4 5 6 7 8 9




Questionnaire

9. Does this object apex or concave? Please give your prefer number.

Extremely Concave Flat Extremely Apex

1 2 3 4 5 6 7 8 9




Questionnaire




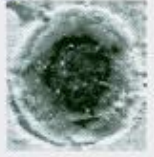
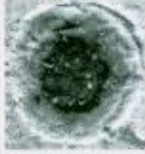
10. Does this object apex or concave? Please give your prefer number.

Extremely Concave Flat Extremely Apex

1 2 3 4 5 6 7 8 9



Crater 3

Questionnaire	Questionnaire
<p>11. Does this object apex or concave? Please give your prefer number.</p> <p>Extremely Concave Flat Extremely Apex</p> <p>1 2 3 4 5 6 7 8 9</p> 	<p>12. Does this object apex or concave? Please give your prefer number.</p> <p>Extremely Concave Flat Extremely Apex</p> <p>1 2 3 4 5 6 7 8 9</p> 
<p>13. Does this object apex or concave? Please give your prefer number.</p> <p>Extremely Concave Flat Extremely Apex</p> <p>1 2 3 4 5 6 7 8 9</p> 	<p>14. Does this object apex or concave? Please give your prefer number.</p> <p>Extremely Concave Flat Extremely Apex</p> <p>1 2 3 4 5 6 7 8 9</p> 
<p>15. Does this object apex or concave? Please give your prefer number.</p> <p>Extremely Concave Flat Extremely Apex</p> <p>1 2 3 4 5 6 7 8 9</p> 	<p>The End</p> <p>• Thank You!</p>